



HAL
open science

Insights into pyrolysis kinetics of xylene isomers behind reflected shock waves

Wenyu Sun, Alaa Hamadi, Fabian E Cano Ardila, Said Abid, Nabiha Chaumeix, Andrea Comandini

► **To cite this version:**

Wenyu Sun, Alaa Hamadi, Fabian E Cano Ardila, Said Abid, Nabiha Chaumeix, et al.. Insights into pyrolysis kinetics of xylene isomers behind reflected shock waves. *Combustion and Flame*, 2022, 244, pp.112247. 10.1016/j.combustflame.2022.112247 . hal-03747035

HAL Id: hal-03747035

<https://hal.science/hal-03747035v1>

Submitted on 7 Aug 2022

HAL is a multi-disciplinary open access archive for the deposit and dissemination of scientific research documents, whether they are published or not. The documents may come from teaching and research institutions in France or abroad, or from public or private research centers.

L'archive ouverte pluridisciplinaire **HAL**, est destinée au dépôt et à la diffusion de documents scientifiques de niveau recherche, publiés ou non, émanant des établissements d'enseignement et de recherche français ou étrangers, des laboratoires publics ou privés.



Contents lists available at ScienceDirect

Combustion and Flame

journal homepage: www.elsevier.com/locate/combustflame

Insights into pyrolysis kinetics of xylene isomers behind reflected shock waves

Wenyu Sun^{a,1,2,*}, Alaa Hamadi^{a,2}, Fabian E. Cano Ardila^a, Said Abid^{a,b}, Nabiha Chaumeix^a, Andrea Comandini^{a,*}

^a CNRS-INSIS, I.C.A.R.E, 1C, Avenue de la recherche scientifique, 45071 Orléans cedex 2, France

^b Université d'Orléans, 6 Avenue du Parc Floral, 45100 Orléans, France

ARTICLE INFO

Article history:

Received 12 September 2021

Revised 7 June 2022

Accepted 8 June 2022

Available online 24 June 2022

Edited by Prof. Perrine Pepiot

Keywords:

Xylenes

Pyrolysis

Single-pulse shock tube

Kinetic modeling

Polycyclic aromatic hydrocarbon (PAH)

ABSTRACT

This work reports a kinetic study on the pyrolysis of three xylene isomers based on single-pulse shock tube experiments and detailed kinetic modeling. Speciation measurements for the post-shock gas mixtures are obtained via sampling and gas-chromatography-mass spectrometry over a temperature range of 1150–1650 K at a nominal pressure of 20 bar. A sub-mechanism incorporating consumption reactions of xylene isomers as well as subsequent pathways leading to polycyclic aromatic hydrocarbons (PAHs) is developed and integrated into our on-going PAH formation kinetic model. The model can satisfactorily predict the qualitative measurements and accurately characterize both the similarities and fuel-specific features in the pyrolysis of three xylenes. The three isomers decompose at similar rates, though m-xylene exhibits a slightly weaker reactivity. This arises from the fact that m-xylyl, different from its o- and p- counterparts, cannot undergo hydrogen loss to form m-xylylene diradical. Distinct consumption schemes of the three xylyl radicals also result in the different species pools observed at temperatures below 1400 K. A large amount of styrene results from a stepwise isomerization of o-xylylene following dehydrogenation of o-xylyl. An early formation of anthracene is noted as a unique phenomenon in o-xylene pyrolysis, which is attributed to specific reactions of o-xylyl. Due to a relatively high abundance of m-xylyl, the self-recombination product 3,3'-dimethylbibenzyl is among the major species formed at the initial stage of m-xylene pyrolysis. p-Xylyl predominantly converts to p-xylylene which is largely consumed via polymerization processes. Besides, mutual conversions among the three xylyl radicals are found to play an essential role in the pyrolysis of three xylenes. Toluene is measured of significant concentrations in the pyrolysis of all three isomers, which rationalizes that PAH speciation in the pyrolysis of three xylenes and toluene is highly similar at elevated temperatures. Modeling analyses show that apart from the benzyl/toluene chemistry, reactions involving C₈ species also have important contributions to PAH formation in xylenes pyrolysis.

© 2022 The Author(s). Published by Elsevier Inc. on behalf of The Combustion Institute. This is an open access article under the CC BY license (<http://creativecommons.org/licenses/by/4.0/>)

1. Introduction

Xylenes are found as important components in crude oils and also widely used to formulate surrogates for liquid transportation fuels [1–3]. Predictive combustion kinetic models for xylenes consumption and the subsequent formation of pollutants such as polycyclic aromatic hydrocarbons (PAHs) are highly necessary towards

practical applications. Plenty of kinetic investigations on one or more xylene isomers under different combustion relevant conditions are available in literature. Fundamental combustion experiments for the xylene isomers have been carried out using various facilities, including flow-reactor [4–6], jet-stirred reactor (JSR) [7–9], shock tubes [10–13], rapid compression machine [14,15] and flames [6,16–22]. Among these studies, advanced speciation diagnostics were implemented. In particular, synchrotron based mass spectrometry and imaging photoelectron photoion coincidence (iPEPICO) spectroscopy techniques were employed to obtain quantitative measurements for reactive combustion/pyrolysis products [6,18,19] and to unambiguously resolve isomers [22–24]. Ab-initio calculations [25,26] were also carried out to derive rate coefficients for reactions of xylenes and relevant radicals, which laid

* Corresponding authors.

E-mail addresses: sunwenyu0702@gmail.com (W. Sun), andrea.comandini@cnrs-orleans.fr (A. Comandini).

¹ Current address: Materials Science Division, Lawrence Livermore National Laboratory, Livermore, CA 94551, United States of America.

² Both authors have equally contributed to this work.

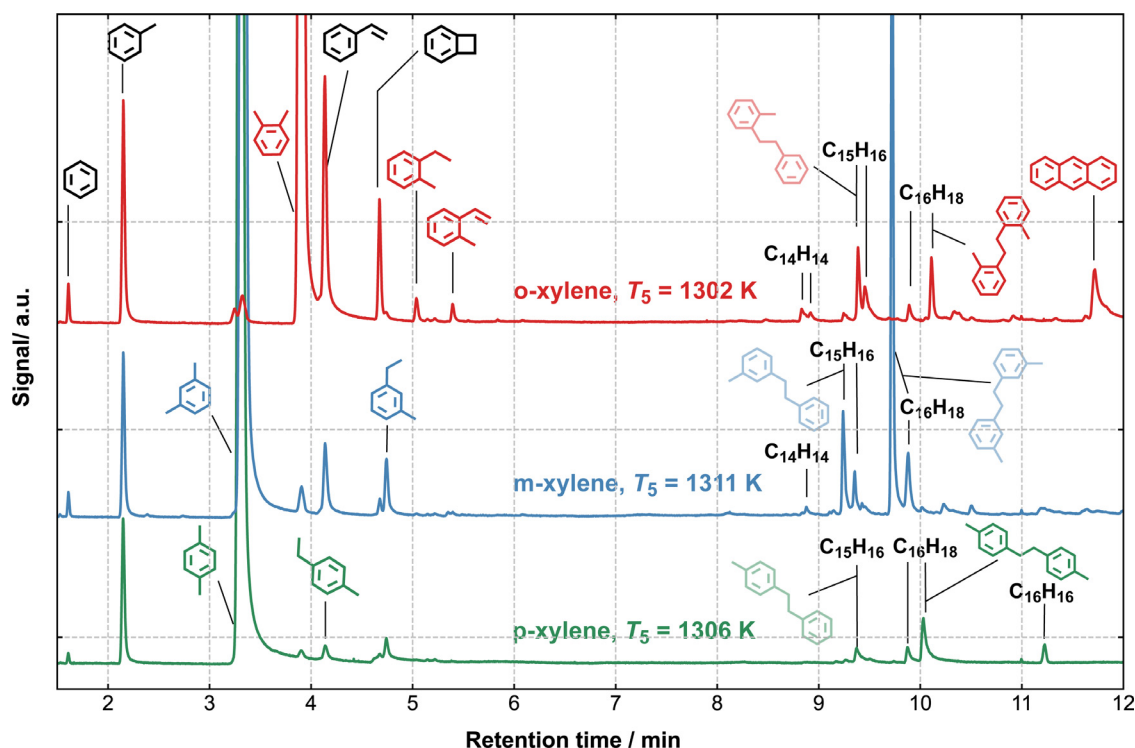


Fig. 1. Signals recorded by the first GC in the pyrolysis of three xylene isomers at the temperature around 1300 K.

essential foundation for the development and optimization of detailed combustion kinetic models for xylenes.

PAH formation kinetics is an important aspect of combustion properties of aromatic fuels, and specific reaction pathways can be highlighted under pyrolysis conditions. However, most of the above-mentioned studies addressed reaction kinetics of xylenes under oxidation conditions, while pyrolysis studies, especially those involving comprehensive speciation measurements and comparisons among the three isomers, are scarce. Rate coefficients for the initial thermal decomposition steps of xylenes and xylil radicals were derived from a few early shock tube studies [27–30]; A very recent work by Yuan *et al.* [6] reported detailed species mole fractions measured from *o*-xylene pyrolysis in a flow tube at low- and atmospheric pressures. Regarding the comparison among the three xylenes, *o*-xylene was consistently observed of higher reactivity than the *m*- and *p*- isomers, in terms of higher flame propagation speeds [17,21] or shorter ignition delay time [12]; under pyrolysis conditions, it was only mentioned by da Costa *et al.* [29] that the three isomers have similar decomposition rates, while detailed speciation behaviors have not been compared to the best of our knowledge. Comparative studies benefit an in-depth understanding of how the fuel structural features correlate to combustion properties. It is shown that the methylation on the aromatic ring makes the combustion properties, such as decomposition reactivity and sooting tendency, of toluene significantly different from those of benzene [31]. As for xylene molecules where two methyl groups are present on the benzene ring, it is important to reveal how an extra methyl substitution changes the reaction pathways in comparison to toluene and how the relative position of the two methyl groups brings further influences under pyrolysis conditions.

To this end, the current work focuses on a comparative study for the pyrolysis of three xylenes. Experiments are performed with a single-pulse shock tube over a temperature range of 1150–1650 K at a nominal pressure of 20 bar. The high-pressure condition is chosen to be more relevant to practical operations. Samples are withdrawn from post-shock gas mixtures and ana-

lyzed through the gas-chromatography (GC)/GC-mass spectrometry (MS) technique, yielding temperature dependent mole fractions for a variety of species up to four ring PAHs. Updates for xylene reactions are made to a kinetic model which has been developed in our serial works [31–36] to predict the PAH formation from the pyrolysis of practical fuel components and mixtures. Satisfactory predictive performances for the experimental results are achieved by the kinetic model. Further modeling analyses are thus used to identify crucial reactions or processes that affect fuel decomposition reactivity and speciation behaviors in the pyrolysis of individual xylene isomers, and to interpret fuel-specific and common phenomena in all three cases.

2. Shock tube pyrolysis experiments

The experimental work is carried out with the single-pulse shock tube facility at ICARE, Orléans. The details about the shock tube and the coupled GC/GC–MS speciation diagnostic techniques have been well documented in our previous publications [31,32,34]. Briefly, the driven section of the shock tube, with a length of 6.0 m and an inner diameter of 78 mm, is separated from the driver section by a double diaphragm section. To run the shock tube in a single-pulse fashion, a dump tank, with a volume five times larger than the driven section, is placed near the diaphragm on the driven section side. The driven section is heated up at 90 °C to avoid condensation and absorption of fuels or heavy products on the inner surface. Four pressure sensors (CHIMIE METAL A25L05B) are mounted along the sidewall at an interval of 150 mm, with the last one being 82 mm away from the endwall. The recorded pressure signals are used to derive the velocity of the incident shock wave which is further used to compute the post-shock conditions T_5 and p_5 by solving the conservation equations with the ideal gas law and variable heat capacity ratio. This method has been proven to give accurate thermodynamic conditions behind the reflected shock waves for defined shock wave speeds and initial conditions. For each experiment the time-history pressure profile is also provided for accurate simula-

tion of the results. A different method to derive T_5 in single-pulse shock tube experiments adopted by various research groups involves the use of chemical thermometers to derive averaged temperatures throughout the entire reaction process [37]. Such method compensates for the non-idealities encountered in the experimental measurement, but it is subject to certain uncertainties related to: i) the measurement of the incident shock wave velocity; ii) the definition of the unimolecular reaction rate constant parameters for the selected species; iii) extrapolation of the calibration curves outside the temperature range of the chemical thermometers (valid mainly for temperatures higher than 1350–1400 K. In addition, previous studies have shown how the use of chemical thermometers [38,39] or constant pressure conditions cannot correctly account for the reactions involving the resonantly-stabilized radicals [33–36,40]. Considering that the present work is performed with a shock tube of large bore where the non-idealities are minimized, the current method based on the theoretical T_5 calculation is preferred here. The physical dimension of the pressure sensors introduces uncertainties in the correlation between the time when the pressure rise is observed and the corresponding location on the sensitive area of the sensors. The sensitive area extends around ± 1 mm with respect to the center of the sensor, thus the maximum error in the distance between two adjacent sensors is 2 mm. An uncertainty of ± 30 K is estimated in the calculated T_5 . A PCB Piezotronics pressure sensor, shielded by a layer of room-temperature vulcanizing (RTV) silicone, is mounted on the endwall to measure the local pressure history. The reaction time for each experiment is defined as the time interval between the arrival of the incident shock wave and the time point when the pressure decreases to 80% p_5 due to the quenching rarefaction waves. Exemplary pressure history traces are provided in Fig. S1 in the **Supplemental Material** to illustrate how the corresponding reaction time is defined. The nominal reaction time is 4.0 ms using the current experimental configuration. An air actuated valve is located at the center of the endwall to sample the post-shock gas mixtures. The operation of the sampling valve is triggered by the endwall pressure signal with a delay set at 4.0 ms (equivalent to the nominal reaction time) to account for the reaction duration. The opening and closing of the valve take hundreds of milliseconds, and the relatively long process is due to the mechanical restrictions. Gas samples with large volumes are sampled, so that PAHs at trace levels (~ 0.01 ppm) can be detected in our experiments. The sampled gas mixtures are sampled via SilcoTek tubes, which are heated at 250 °C to avoid condensation, to the GC injection system. Two GCs are placed in series, in charge of measuring different types of products. The first GC (Agent 7890) is equipped with a flame ionization detector (FID) connected to a DB-17-ms column, to separate and detect PAHs. A thermal conductivity detector (TCD), together with a Molsieve 5A column, is employed to monitor the absence of air. An external valve box, which can regulate the temperature up to 320 °C, is used to place the injection system of this GC, to minimize the loss of heavy species due to condensation or absorption during sample storage and injection. For the second GC (Thermo Trace GC Ultra), an FID connected to an HP-PLOT Q column is installed to measure the small C_1 – C_4 hydrocarbons and monocyclic aromatics. A DSQ™ (dual stage quadrupole) mass spectrometer is also used to assist the identification of PAH products.

The PAHs are mainly identified according to their retention time that is known from prior injection of standards. Most PAH products were already observed in our previous works which accumulated the knowledge of retention times for dozens of PAH compounds [31–36,41]. The retention time of some specific standards that are considered as candidates of observed products are newly obtained in the present work and provided in **Table S1**. Other crucial information, such as the elemental composition of a specific peak, is provided by the mass spectrometer which also proposes

possible candidates available in the NIST library. **Figure 1** shows the signals recorded by the first GC in the pyrolysis of three xylene isomers at around 1300 K, at which about 20% of the fuel is consumed in each case. We choose to show the signals at this temperature mainly because the PAHs specific in xylenes pyrolysis have considerable concentrations, and they are not significantly influenced by the peaks of PAHs formed at elevated temperatures. Apart from the regular products including benzene, toluene and styrene, which are usually present among the products in our previous experiments, benzocyclobutene is observed for the first time in the current work. C_9H_{12} peaks are detected at a similar retention time with benzocyclobutene in the pyrolysis of all three xylene isomers. Given that both ethylbenzene and xylenes were produced in toluene pyrolysis [35], C_9H_{12} peaks might be contributed by ethyltoluene and trimethylbenzene isomers. Standards of all six isomers (2-, 3- and 4- ethyltoluenes and 1,2,3-, 1,3,4- and 1,3,5- trimethylbenzenes) were injected and the signals were compared with the experiments, as presented in **Fig. S2**. It is confirmed that ethyl-toluene isomer is formed in the pyrolysis of each xylene, while trimethylbenzenes are absent or negligible in the current experiments. It is noteworthy that three bunches of peaks, with the respective formulas of $C_{14}H_{14}$, $C_{15}H_{16}$ and $C_{16}H_{18}$, are formed at a relatively low temperature regime where xylenes start to decompose. Among these peaks, a $C_{16}H_{18}$ and a $C_{15}H_{16}$ species have remarkable intensities in separate cases. They are assumed to be formed through the corresponding xylyl self-recombination and the xylyl + benzyl recombination, respectively. The existence of 2,2'-dimethyl-bibenzyl in o-xylene pyrolysis and 4,4'-dimethyl-bibenzyl in p-xylene pyrolysis are further confirmed by their retention time. The presence of other species, as shown in lighter colors in **Fig. 1**, cannot be unambiguously verified due to the unavailability of the corresponding standards. A considerable amount of anthracene is noticed at the beginning of o-xylene decomposition.

Species quantification requires calibration experiments for the FID responses. C_1 – C_4 hydrocarbons (except diacetylene) and small aromatics including benzene, toluene, ethylbenzene, styrene, phenylacetylene, benzocyclobutene and xylene isomers are calibrated using gas mixtures with known compositions. Diacetylene (C_4H_2) is calibrated through high-temperature acetylene pyrolysis experiments based on the carbon atom balance. Specific procedures are followed to calibrate PAH species, as detailed in [34–36]: i) the targeted PAH standards in condensed phase are dissolved in dichloromethane to prepare calibration solutions with desired PAH concentrations; ii) a small doze (a few microliters) of the solution is injected through a septum on the sidewall of a glass vessel which is previously vacuumed and heated up at 150 °C; iii) upon the immediate vaporization of the solution, the vessel is filled with argon to a pressure around 1.2 bar. The gas mixture stays for about 15 min to homogenize and the concentrations of the PAHs can be calculated; iv), the calibration gas mixture is injected into the GC at least three times to test the reproducibility of the measurement and to obtain the pressure-normalized FID responses for the PAHs. The above steps are repeated using gas mixtures containing different concentrations of targeted PAHs, so that the calibration factors can be derived. For the PAHs up to three rings, the regressions of the normalized signal-concentration plots have good linearity. This method, however, cannot well apply to larger PAHs, and the possible reason is that the complete vaporization of the four-ring and larger PAHs cannot be guaranteed. The calibration factors for four ring PAHs (pyrene and fluoranthene) are extrapolated using those of one- to three- ring aromatics (benzene, naphthalene and phenanthrene). The errors in the calibration factors are the main uncertainty source of the measured species mole fractions. Uncertainty factors are estimated to range from 5% to 10% for the species directly calibrated in gas-phase, and 10–15% for the PAHs that are experimentally calibrated. The measuring errors may increase to

Table 1
Compositions of the experimental gas mixtures analyzed by the GC.

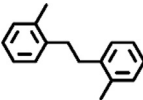
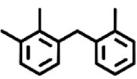
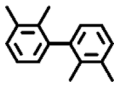
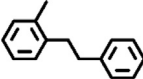
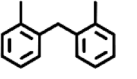
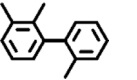
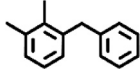
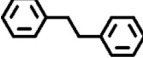
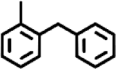
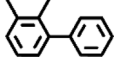
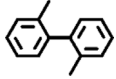
	Fuel	Impurities
o-xylene	113 ppm	m-xylene: 0.27 ppm
m-xylene	106 ppm	o-xylene: 0.28 ppm
p-xylene	101 ppm	o-xylene: 0.10 ppm

20–50% or even more for the PAHs without experimental calibration factors.

Chemicals used in the current experiments, including the fuels (xylenes, with purities $\geq 99.0\%$) and the PAH standards, are purchased from Sigma-Aldrich. The bath gas argon ($>99.9999\%$) and the driven gas helium ($>99.995\%$) are supplied by Air-Liquide. A 136 L electropolished stainless steel cylinder is used to prepare experimental gas mixtures containing around 100 ppm xylene isomers. The liquid fuel (degassed using liquid nitrogen) is introduced to the cylinder which is previously vacuumed to a pressure below 10^{-5} mbar using a molecular turbo pump. The partial pressure of the fuel vapor is monitored by a MKS Baratron pressure transducer (model 122BA) with the range of 0–10 Torr. The cylinder is then filled with argon to a total pressure around 10 bar, measured by a 0–10,000 Torr MKS Baratron pressure transducer (model 627D). The prepared gas mixtures stay overnight before experiments to ensure good homogeneity. Exact compositions of the experimental mixtures are analyzed by the GC, and the major impurities are found as other xylene isomers in each case. The compositions of the experimental mixtures are listed in Table 1. The pressure in the driven section of the shock tube is pumped to below 10^{-5} mbar before being filled with the experimental mixture in each operation. Carbon deposits on the inner surface of the driven section is cleaned every day after the experiments. The three sets of experimental results obtained in the current work are provided in the **Supplementary Material**, including the post-shock conditions T_5 , p_5 , the measured pressure profiles, the defined reaction time, as well as species mole fractions in each experiment.

Table 2

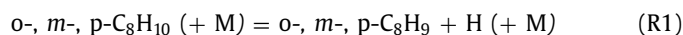
Possible structures for the $C_{16}H_{18}$, $C_{15}H_{16}$ and $C_{14}H_{14}$ isomers detected in the current experiments. The potential formation reactions and their nomenclatures in the kinetic model are provided. Except 2,2'-dimethylbibenzyl (o- $C_{16}H_{18}$), 3,3'-dimethylbibenzyl (m- $C_{16}H_{18}$), 4,4'-dimethylbibenzyl (p- $C_{16}H_{18}$) and bibenzyl ($C_6H_5C_2H_4C_6H_5$), other species are lumped isomers with different methyl substitution positions.

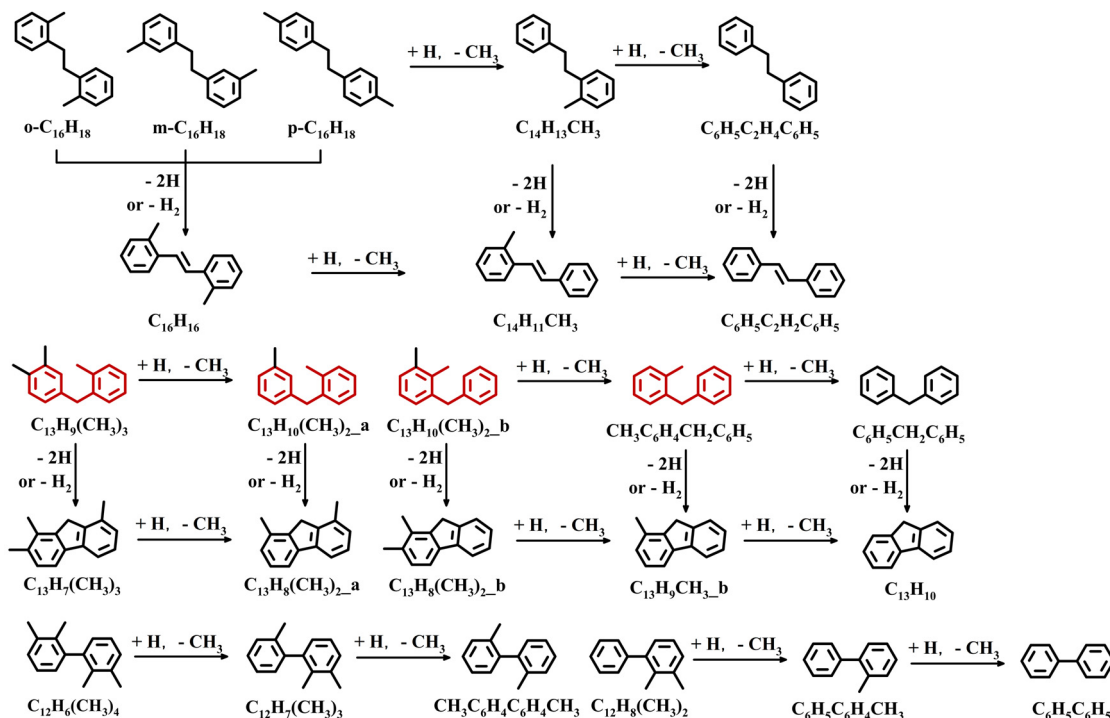
Formula	Bibenzyl-centered	Diphenylmethane-centered	Biphenyl-centered
$C_{16}H_{18}$	2o-, m-, p- C_8H_9 = o-, m-, p- $C_{16}H_{18}$ 	o-, m-, p- C_8H_9 + o-, m-, p- $CH_3C_6H_3C_6H_3$ = $C_{13}H_9(CH_3)_3$ 	2o-, m-, p- $CH_3C_6H_4CH_3$ = $C_{12}H_6(CH_3)_4$ 
$C_{15}H_{16}$	o-, m-, p- C_8H_9 + C_7H_7 = $C_{14}H_{13}CH_3$ 	o-, m-, p- C_8H_9 + $CH_3C_6H_4$ = $C_{13}H_{10}(CH_3)_2$ _a  o-, m-, p- $CH_3C_6H_3C_6H_3$ + C_7H_7 = $C_{13}H_{10}(CH_3)_2$ _b 	o-, m-, p- $CH_3C_6H_3CH_3$ + $CH_3C_6H_4$ = $C_{12}H_7(CH_3)_3$ 
$C_{14}H_{14}$	C_7H_7 + C_7H_7 = $C_6H_5C_2H_4C_6H_5$ 	o-, m-, p- C_8H_9 + C_6H_5 = $CH_3C_6H_4CH_2C_6H_5$ C_7H_7 + $CH_3C_6H_4$ = $CH_3C_6H_4CH_2C_6H_5$ 	$CH_3C_6H_3C_6H_3$ + C_6H_5 = $C_{12}H_8(CH_3)_2$  $CH_3C_6H_4$ + $CH_3C_6H_4$ = $CH_3C_6H_4C_6H_4CH_3$ 

3. Kinetic modeling

A kinetic model has been developed in our serial works [31–36], with a major aim of accurately predicting the PAH speciation in combustion/pyrolysis of practical fuels and fuel mixtures. The reaction kinetics of xylenes has not been examined and addressed yet in our previous studies. Thus, the sub-mechanism for xylenes in earlier versions of the kinetic model is kept original as in the CRECK model [42] which we started the model development with. In the present work, the lumped species (XYLENE) is separated into three isomers, o-, m- and p-xylene (o-, m- and p- C_8H_{10}), for which the corresponding reaction mechanisms are constructed based on uniform rate rules or theoretical and kinetic modeling works in literature.

Given that xylenes share similarities with toluene for which the reaction mechanism has been well established, a part of reactions for xylenes and the corresponding rate coefficients in the current model are evaluated through analogies to toluene reactions. Specifically, for xylene unimolecular decomposition reactions, including the benzylic C–H bond fission (R1), C–C bond fission resulting in methyl phenyl ($CH_3C_6H_4$) (R2), and C–H bond fission on the benzene ring (R3), rate coefficients of the corresponding toluene reactions, which originate from the theoretical work by Klippenstein et al. [43], are used. For bimolecular reactions, mainly the two types of hydrogen abstraction reactions (R4 and R5) and the *ipso*-substitution reactions forming toluene (R6), the rate coefficients of toluene reactions are adopted with consideration of the changed degeneracy for xylenes.





Scheme 1. Demethylation and dehydrogenation processes and starting from the $C_{16}H_{18}$ isomers formed from xylenes pyrolysis.

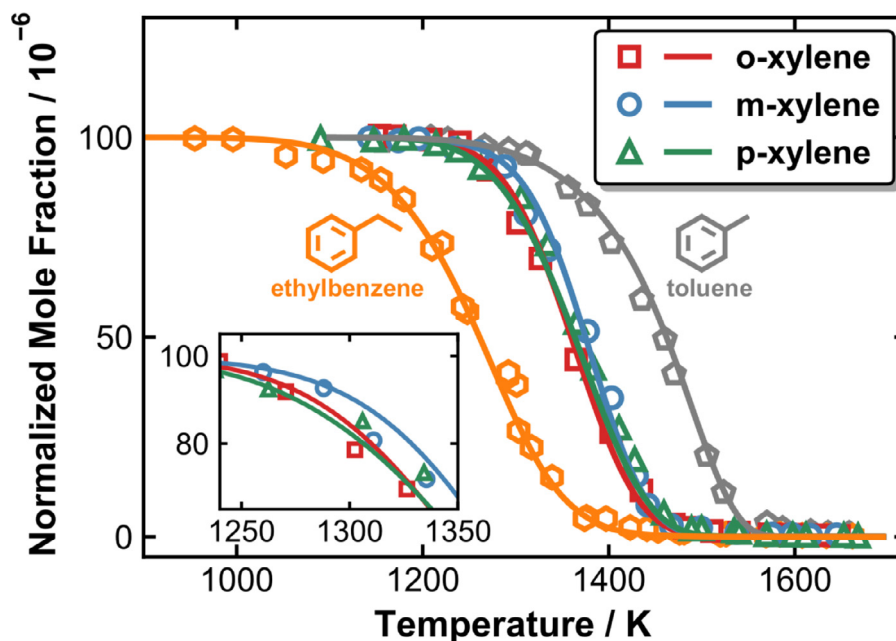
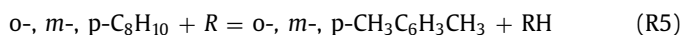
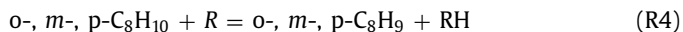


Fig. 2. Measured (symbols) and simulated (solid lines) mole fractions for xylene isomers, and the fuel mole fraction profiles in toluene [35] and ethylbenzene [33] pyrolysis under similar conditions are also shown for comparison. Initial fuel mole fractions are all normalized to 100 ppm.



The major products of the above reactions include fuel radicals, xylyl and dimethyl-phenyl isomers, toluene and benzyl. The

sub-mechanisms for toluene and benzyl, including their dissociation processes and the interactions with other combustion intermediates such as C_2 and C_3 , have been addressed in our previous works [31,34,35]. Xylyl radicals are resonantly stabilized and with benzylic radical sites, so they resemble benzyl in the consumption reactions in our kinetic model. *o*-xylyl ($o-C_8H_9$) and *p*-xylyl ($o-C_8H_9$) predominantly decompose to *o*-xylylene ($o-C_8H_8$) + H and *p*-xylylene ($p-C_8H_8$) + H, respectively (R7). The rate constants measured by Fernandes et al. [30] are adopted. Differently, *m*-xylyl ($m-C_8H_9$) cannot undergo the hydrogen loss forming the unstable

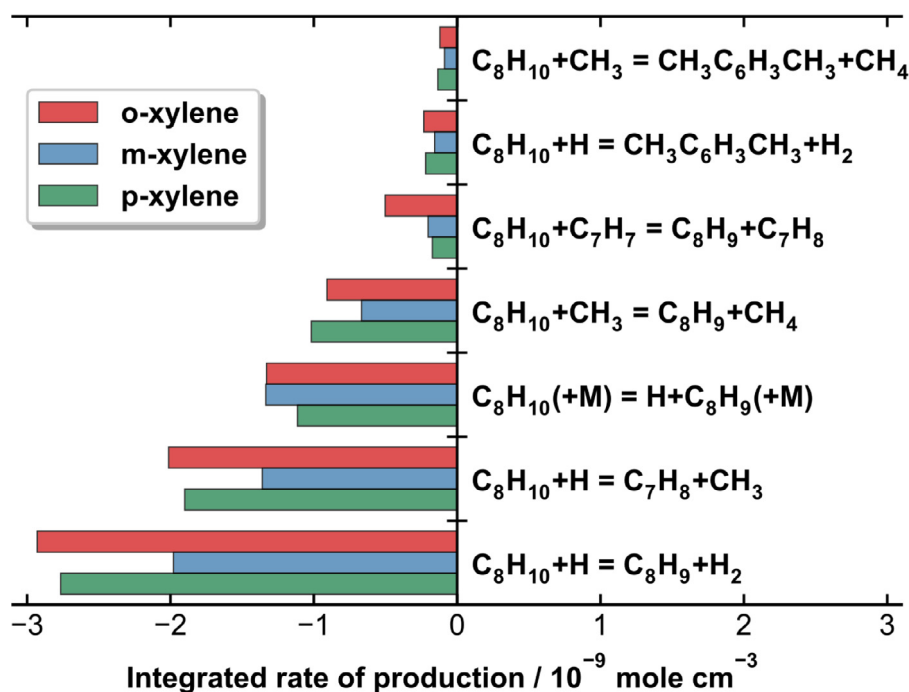


Fig. 3. Integrated ROP coefficients for fuels in the pyrolysis of xylene isomers at $T_5 = 1350$ K.

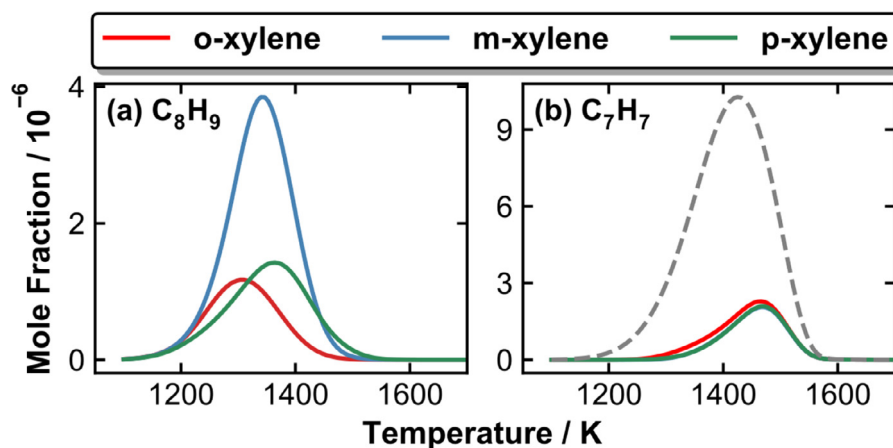
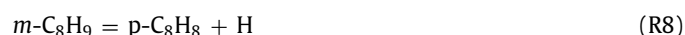


Fig. 4. Simulated mole fraction profiles of (a) xylyl radicals (o - C_8H_9 , m - C_8H_9 and p - C_8H_9) and (b) benzyl (C_7H_7) in the pyrolysis of three xylene isomers. The dashed line is the simulated C_7H_7 mole fraction profile in 100 ppm toluene pyrolysis.

biradical m -xylylene, as proven via experimental [22–24] and theoretical [25] approaches. The rearrangement to o - and p - isomers (o - C_8H_9 and p - C_8H_9) are potential consumption channels. p - C_8H_8 was observed among the products of m - C_8H_9 decomposition [22–24]. Therefore R8, with the rate coefficient reported by da Silva et al. [25], is used to depict the processes of m - C_8H_9 converting to p - C_8H_9 which further decomposes. The detection of benzocyclobutene ($C_6H_4C_2H_4$) [22] in m - C_8H_9 consumption may serve as an indirect evidence of the isomerization of m - C_8H_9 to o - C_8H_9 . A reaction potential energy surface at the G4 level of theory shows that the re-arrangements of m - C_8H_9 to o - C_8H_9 and p - C_8H_9 follow similar processes and the highest energy barriers are both around 70 kcal/mol [23]. The mutual conversion between o - C_8H_9 and p - C_8H_9 was also proposed by Hemberger et al. [24], and recently, Yuan et al. [19] observed o - C_8H_9 and o - C_8H_8 in premixed flames fueled by p - C_8H_{10} . R9 and R10 are included in the current model to account for the mutual conversions among the xylyl isomers, and the rate coefficients are taken from the kinetic models by Yuan et al. [6,19]. Alternative decomposition pathways of xylyl rad-

icals are also considered in the current kinetic model. Analogous to benzyl decompositions to fulvenallene (C_7H_6) + H and o -benzyl (o - C_6H_4) + CH_3 , the decomposition of xylyl radicals can lead to methyl-fulvenallene ($C_7H_5CH_3$) + H and C_7H_6 + CH_3 , respectively. The reaction channels leading to cyclopentadiene (C_5H_6) + propargyl (C_3H_3) and methyl-cyclopentadienyl ($C_5H_4CH_3$) + C_2H_2 proposed by Gail and Dagaut [7–9] are also included in the current model.



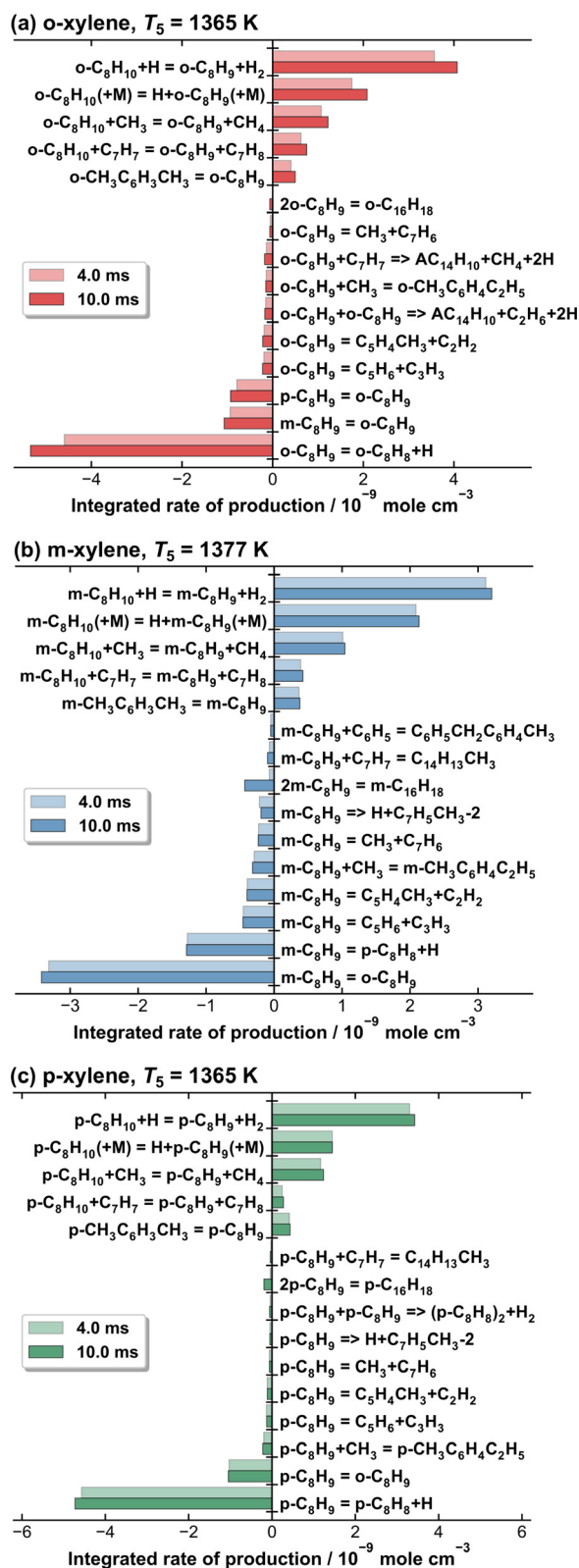
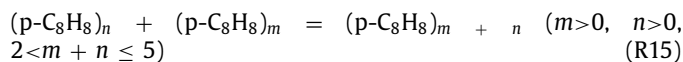
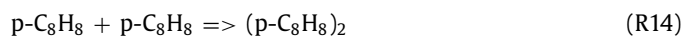


Fig. 5. Integrated ROP coefficients for (a) o-C₈H₉ in o-xylene pyrolysis at T_5 of 1365 K, (b) m-C₈H₉ in m-xylene pyrolysis at T_5 of 1377 K and (c) p-C₈H₉ in p-xylene pyrolysis at T_5 of 1365 K. The ROP analyses are performed using two different methods: by assuming a constant pressure of 20 bar over a nominal reaction time of 4.0 ms and by using the measured pressure profile up to 10 ms.

The stepwise isomerization of o-xylylene (o-C₈H₈) → C₆H₄C₂H₄ → styrene (C₆H₅C₂H₃) (R11 and R12) has been established as the major route leading to o-C₈H₈ consumption. o-C₈H₈ may also convert to C₆H₅C₂H₃ bypassing the intermediate C₆H₄C₂H₄ (R13), and this process involves multiple steps such as biradical formation, closure of a three-membered ring and ring expansion [24]. The rate constant for the o-C₈H₈ to C₆H₄C₂H₄ isomerization (R11), $k_{11} = 2.52 \times 10^{12} \text{ s}^{-1} \exp(29,354 \text{ cal/mol} / RT)$, comes from a recent theoretical work [44]. The same A factor is used for R13, for which the Ea is set as the maximum energy barrier (57.8 kcal/mol) in the process, i.e. the formation of a biradical [24]. The experimentally derived rate coefficient from [45] is used for R12. Other possible consumption pathways of C₆H₄C₂H₄ that appear on the reaction PES in [24] are also considered, such as dissociation to o-C₆H₄ + C₂H₄, dehydrogenation reactions forming C₆H₄C₂H₃ radical and benzocyclobutadiene (C₆H₄C₂H₂).



Different from o-C₈H₈, the main product of p-C₈H₉ decomposition, p-C₈H₈, cannot undergo the isomerization forming a four-membered ring. As mentioned above, a C₁₆H₁₆ species is observed as one of the main aromatic products at the initial stage of p-C₈H₁₀ decomposition, which is not observed in the cases of o- and m-C₈H₁₀. It was mentioned in an early study [46] that the accumulated p-C₈H₈ could rapidly polymerize to give poly-(p-xylylene). Despite the lack of further evidence, we assume that the C₁₆H₁₆ peak with the retention time of 11.2 min (see Fig. 1) corresponds to a polymer containing two p-C₈H₈ units (p-C₈H₈)₂. Larger polymers perhaps exist in condensed phase and cannot be detected by the GC in the current experiments. The polymerization of p-C₈H₈ are considered as irreversible processes in the current model, since the formed larger polymers may leave the gas-phase sample, and the reactions R14 and R15 are used to describe the polymerization processes forming polymers containing up to five p-C₈H₈ units. The rate constant of the polymerization of ethylene (C₂H₄+C₂H₄ = C₄H₈) [47] is used for each reaction.



The minor fuel radicals dimethyl-phenyl radicals (o, m, and p-CH₃C₆H₃CH₃) are actually lumped species in individual cases. Rate coefficients for the isomerization reactions (R16) to more stable radicals of benzylic nature are from a theoretical work by Dames and Wang [26]. The abundance and long lifetime of xylyl radicals allow their interactions with other intermediates such as the abundant C₁-C₃ species. Similar to the ethylbenzene (C₆H₅C₂H₅) formation from C₇H₇ + CH₃ recombination, xylyl radical may combine with CH₃, forming ethyl-toluene isomers (R17). The reactions of C₇H₇ with C₂H₂ and C₃H₃ have been proven as efficient pathways forming indene (C₉H₈) and naphthalene (C₁₀H₈), respectively, in our recent works [34,35]. In a similar manner, the interactions between xylyl radicals and C₂H₂/C₃H₃ potentially lead to methyl-substituted indene/naphthalene (R18 and R19). The product of R18, CH₃C₉H₇, is a lumped species for 4-, 5-, 6-, 7- methyl-indene (with

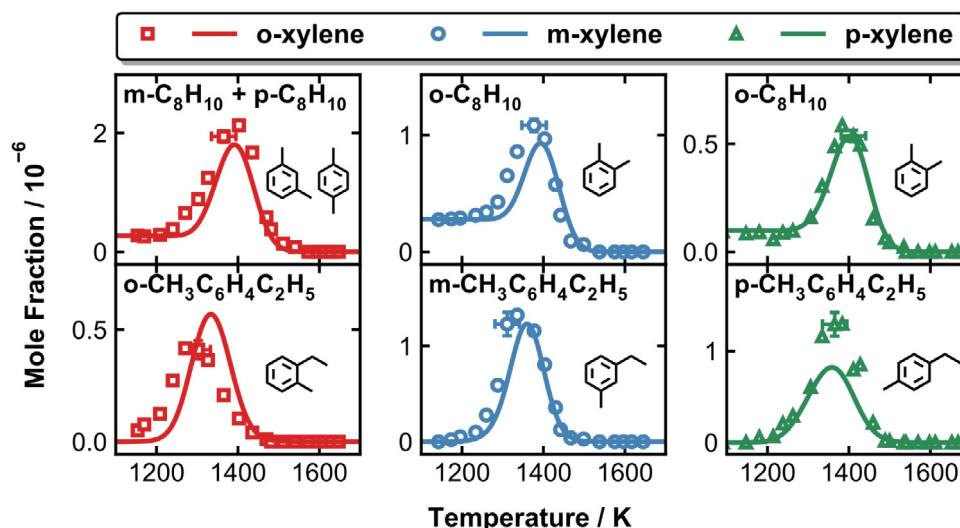
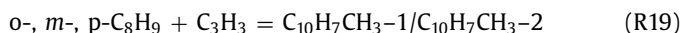
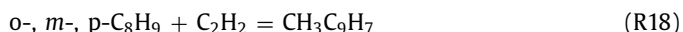
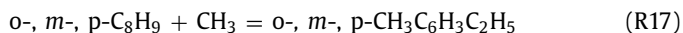
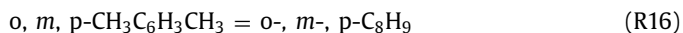


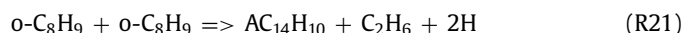
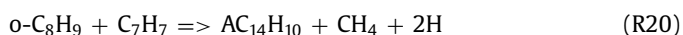
Fig. 6. Measured (symbols) and simulated (lines) mole fraction profiles of fuel-specific MAH intermediates in the pyrolysis of three xylene isomers.

the methyl substitute on the benzene ring). As for R19, by reacting with C_3H_3 , $o-C_8H_9$ and $p-C_8H_9$ can only result in 1-methylnaphthalene ($C_{10}H_7CH_3-1$) and 2-methylnaphthalene ($C_{10}H_7CH_3-2$), respectively, while both methyl-naphthalene isomers can be formed in the case of $m-C_8H_9$.



The reactions among xylene fuel radicals (C_8H_9 and $CH_3C_6H_3CH_3$ radicals) and other major aromatic radicals, such as benzyl (C_7H_7) and phenyl (C_6H_5) are summarized in Table 2. The direct recombination reactions lead to non-fused bicyclic PAHs with structures of methyl-substituted bibenzyls, diphenylmethanes or biphenyls and the chemical compositions of $C_{16}H_{18}$, $C_{15}H_{16}$ and $C_{14}H_{14}$. The most essential reactions involve the participation of resonantly stabilized radicals, *i.e.*, the self-recombination of C_8H_9 radicals and the $C_8H_9 + C_7H_7$ recombination reactions, for which the rate coefficients of $o-C_8H_9$ self-recombination reported in [48] are used. Demethylation via stepwise *ipso*-substitution reactions are included as important consumption pathways of these methyl-substituted non-fused PAHs, as shown in Scheme 1.

The species containing *o*-methyl-diphenylmethane structures, as highlighted in Scheme 1, are deemed as precursors of anthracene ($AC_{14}H_{10}$) [46,49,50]. The stepwise dehydrogenation and demethylation of such species may contribute to $AC_{14}H_{10}$ at elevated temperatures, while $AC_{14}H_{10}$ is observed at relatively low temperatures where $o-C_8H_{10}$ just starts to decompose (see Fig. 1). Therefore, lumped intermediates directly forming $AC_{14}H_{10}$, R20 and R21, are included in the kinetic model to account for the early $AC_{14}H_{10}$ formation in $o-C_8H_{10}$ pyrolysis. Estimated rate constants are used for R20 and R21 to match the measured $AC_{14}H_{10}$ mole fraction profiles. The mechanism for $AC_{14}H_{10}$ formation, in particular the early production in $o-C_8H_{10}$ pyrolysis, warrants comprehensive theoretical investigations in the future.



Thermochemical data for the species involved in xylene reactions are from Burcat's database [51] as well as the theoretical work by da Silva [25] if available. For those absent from the above-mentioned sources, the program THERM [52] is used to compute and fit the thermochemical parameters. The mechanism file and the thermochemical data of the current kinetic model are provided in the **Supplementary Material**. To simulate the experimental results, the homogenous reactor model of software COSILAB [53] is used. Two modes of simulations are performed: by using the constant pressure assumption over a nominal reaction time over 4.0 ms, and by inputting the measured pressure profiles that extend to the post-shock quenching up to 10 ms. It has been justified that the first mode of simulations can well characterize most speciation measurements in single-pulse shock tube experiments where post-shock gas mixtures are sampled [37,54]. Nevertheless, the second simulation mode is highly necessary because resonantly-stabilized radicals, including xylyl isomers and benzyl, are involved in the current studied cases. Radical-radical recombination reactions of these species may continue during the quenching by rarefaction waves, thus impacting the final measurements.

4. Results and discussion

Two main aims are involved in the following discussion. First, predictive performances of the kinetic model will be examined via comparisons between simulated and measured species mole fraction profiles. Second, kinetic insights will be probed from combined experimental evidence and modeling analyses, with emphasis on a few different aspects including the fuel decomposition reactivity, the production of fuel-specific intermediates and the PAH formation behaviors. Explanations will be offered for the similar and unique reaction schemes of the three xylene fuels.

4.1. Fuel decomposition reactivity

Figure 2 displays the mole fractions of the xylene fuels, as a function of the post-shock temperature T_5 . The fuel conversion curves of toluene and ethylbenzene reported in our previous works [33,35] are also shown as references. All initial fuel mole fractions are normalized to 100 ppm to facilitate the comparison. Overall, the decomposition reactivity of xylene isomers falls between that of toluene and ethylbenzene, as can be precisely captured by

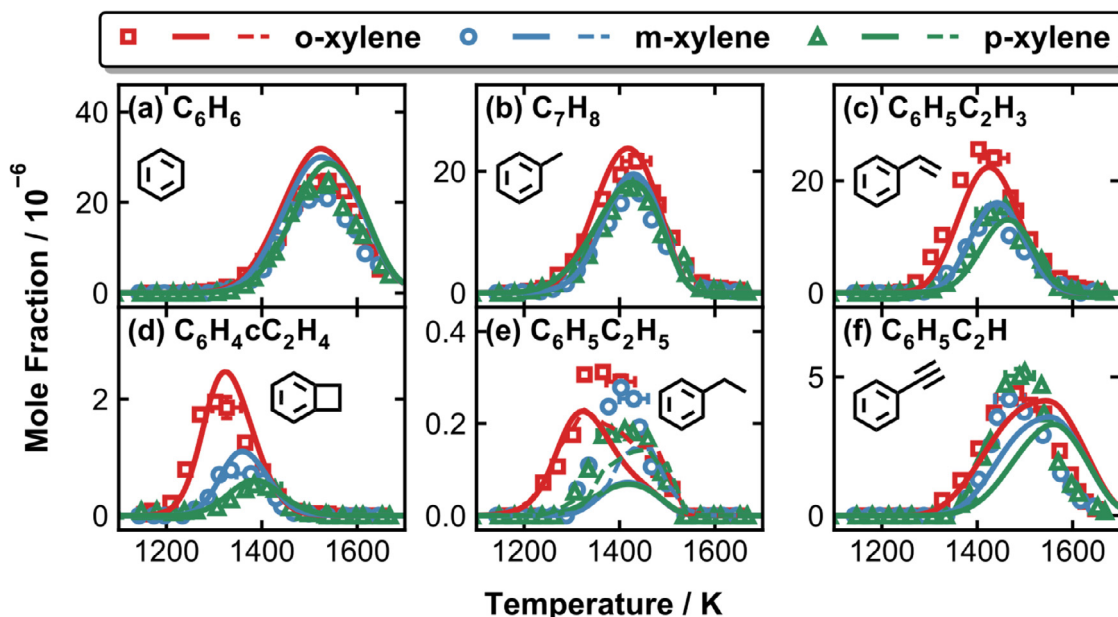


Fig. 7. Measured (symbols) and simulated (solid lines) mole fraction profiles of small hydrocarbons in the pyrolysis of three xylene isomers. The dashed lines in (e) are the ethylbenzene mole fraction profiles simulated using measured pressure profiles.

the current kinetic model. No obvious differences exist among the three isomers, given an uncertainty of ± 30 K in T_5 . The initial stage of xylenes consumption over a temperature range of 1250–1350 K is zoomed in and presented in the inset of Fig. 2. Compared to the other two xylene isomers, m-xylene decomposes at a slightly slower rate, which is consistently shown in both the measurements and simulations. Rate-of-production (ROP) analyses are performed for the fuel in each case at T_5 of 1350 K, where about half of the fuel is consumed, and the integrated ROP coefficients over a nominal reaction time of 4.0 ms are shown in Fig. 3. At the analyzed temperatures, all three xylene isomers decompose dominantly via hydrogen abstraction reactions, mainly by H, CH₃ and C₇H₇, forming xylyl radicals. The *ipso*-substitution reaction forming toluene has the second largest contribution to the consumption of o-xylene and p-xylene, while for m-xylene, both the benzylic C–H bond fission and the *ipso*-substitution have similar importance. Hydrogen abstraction reactions forming dimethyl phenyl radicals also play a minor role in the consumption of xylenes. The reaction schemes of the shown reference fuels, toluene and ethylbenzene, have been discussed before in our recent works [33,35]. The consumption of toluene and ethylbenzene, in comparison to xylene isomers, relies more on unimolecular decomposition reactions, but for different reasons. In the case of toluene pyrolysis, radicals such as H and CH₃ have lower levels, so the importance of bimolecular reactions are relatively inhibited. In a different manner, ethylbenzene unimolecular decomposition via benzylic C–C bond fission and secondary benzylic C–H fission are energetically favored compared to the primary benzylic C–H bond fission in xylenes.

Xylyl radicals and toluene are the major products directly yielded from the decomposition of xylenes. The resonantly stabilized xylyl radicals and benzyl that is further formed through toluene decomposition are expected to play a crucial role in the speciation behaviors of xylenes pyrolysis. Figure 4 compares the simulated mole fractions of xylyls and benzyl among the three cases, and also presents the modeling benzyl mole fraction profile in 100 ppm toluene pyrolysis as a reference. Though hydrogen abstraction reactions from m-xylene proceed at slower rates than those from o- and p- xylenes (see Fig. 3), m-xylyl (m-C₈H₉) has a higher peak concentration than its o- and p- counterparts. Benzyl has a higher speciation temperature window than xylyl radicals,

and it has similar peak concentrations in the pyrolysis of three xylene isomers. Under similar conditions, benzyl produced from toluene pyrolysis has higher concentrations than those of xylyl radicals in the pyrolysis of xylenes. This suggests that xylyl radicals are consumed at higher rates than benzyl, though their formation from xylenes consumption proceeds faster and at lower temperatures. It must be pointed out that the simulated concentrations shown in Fig. 4 are actually extracted at the end of a 4.0 ms reaction duration, where the resonance-stabilized radicals still have relatively high concentrations (a few ppm) in specific temperature regimes. Figure S3 gives the time-dependent mole fraction profiles of the corresponding xylyl radicals in the pyrolysis of xylenes at a temperature around 1370 K (1365 K for o-xylene, 1377 K for m-xylene and 1365 K for p-xylene) simulated using measured pressure profile up to 10 ms. It is seen that the consumption of xylyl radicals extends to the post-shock quenching period, so the relevant reactions can impact the final observed chemical compositions in the sampled post-shock gas mixtures.

ROP-analyzed results of xylyl radicals in corresponding cases at similar T_5 s (1365 K in o-xylene pyrolysis, 1377 K in m-xylene pyrolysis and 1365 K in p-xylene pyrolysis) are presented in Fig. 5. Both analyses at a constant pressure of 20 bar over a nominal reaction time of 4 ms and using the measured pressure profiles up to 10 ms are performed for comparison. The consumption of both o-C₈H₉ and p-C₈H₉ is dominated by the reaction forming the corresponding xylylene (R7). On the other hand, since the hydrogen loss leading to the biradical m-xylylene is not probable, m-C₈H₉ is mainly consumed through the isomerization/rearrangement reactions forming o-C₈H₉ and p-C₈H₈+H. This unique feature explains the lower reactivity of m-xylene than o- and p-xylenes, as a relatively lower amount of H atoms is produced from the initial dissociation steps of m-xylene. Other consumption channels of xylyl radicals include dissociation to small species and recombination reactions with abundant radicals such as methyl, benzyl and xylyls themselves. It is seen that most reactions have higher ROP coefficients in the analyses using measured pressure profiles. This indicates that the consumption of xylyl radicals carry on during the post shock quenching. Among all reactions in the consumption schemes of three xylyl radicals, the self-recombination of m-C₈H₉ forming 3,3'-dimethylbibenzyl (m-C₁₆H₁₈) has the most

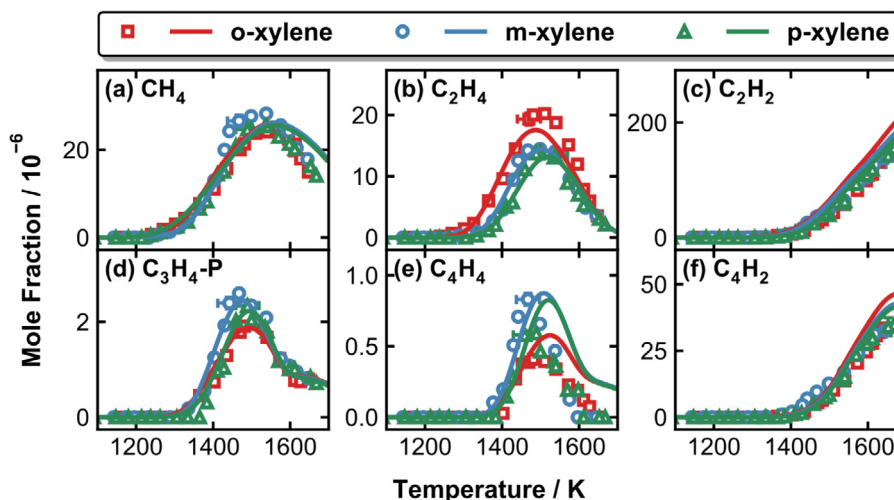


Fig. 8. Measured (symbols) and simulated (lines) mole fraction profiles of small hydrocarbons in the pyrolysis of three xylene isomers.

distinct relative importance when different analyzing methods are used (see Fig. 5(b)).

4.2. Speciation of monocyclic aromatic hydrocarbons (MAHs) and small hydrocarbons

The above ROP analyses for xylyl radicals in individual cases suggest that the mutual conversions are essential consumption channels. As mentioned in the experimental section, small quantities of other xylene isomers exist as impurities in the experimental mixtures, more specifically, m-xylene in o-xylene pyrolysis and o-xylene in m- and p-xylenes pyrolysis (see Table 1). It is found that they are also formed in the experiments. Figure 6 displays the mole fraction profiles of the xylene isomers as impurities/intermediates in each experimental set. The simulations, with the impurities taken into account, agree well the measured profiles: the mole fractions start to increase at around 1250 K, which corresponds to the onset of fuel consumption (see Fig. 2), and reach maxima at approaching 1400 K. The formation of the xylene intermediates relies on the xylyl + H atom recombination reaction, following the fuel radical isomerization. The second row of Fig. 6 displays the mole fraction profiles of the corresponding ethyl-toluene ($\text{CH}_3\text{C}_6\text{H}_4\text{C}_2\text{H}_5$) isomers, which come from the xylyl + methyl recombination reactions. The level of o-ethyl-toluene ($\text{o-CH}_3\text{C}_6\text{H}_4\text{C}_2\text{H}_5$) in o-xylene pyrolysis is relatively lower than those in the cases of m- and p- isomers. This is consistent with the fact that the reaction $\text{o-C}_8\text{H}_9 + \text{CH}_3 = \text{o-CH}_3\text{C}_6\text{H}_4\text{C}_2\text{H}_5$ has a relatively smaller contribution to o-xylyl consumption than m- C_8H_9 /p- $\text{C}_8\text{H}_9 + \text{CH}_3$ reactions in the cases of m-/p-xylyl (see Fig. 5). Though xylyl isomers cannot be detected or quantified in the current experiments, the good predictions for the speciation of xylyl and ethyl toluene intermediates/products proves that the current model well characterize the fates of xylyl radicals under pyrolysis conditions.

Apart from the fuel-specific mono-cyclic aromatic hydrocarbons (MAHs) presented in Fig. 6, some other MAHs that are shared in the species pools of the three cases are also observed. The measured and simulated mole fraction profiles for such species are displayed in Fig. 7. The major MAHs produced in xylene pyrolysis include benzene (C_6H_6), toluene (C_7H_8) and styrene ($\text{C}_6\text{H}_5\text{C}_2\text{H}_3$), with significant peak concentrations of ~ 20 ppm. Benzene (C_6H_6) has similar mole fraction profiles, regarding both sizes and shapes, in the pyrolysis of all three xylene isomers. This is because benzene has a relatively high speciation temperature window, where the fuels are depleted so that the fuel-specific chemistry has lim-

ited influences. The governing formation channels of C_6H_6 are through the consumption reactions of toluene and styrene, more specifically, $\text{C}_7\text{H}_8 + \text{H} = \text{C}_6\text{H}_6 + \text{CH}_3$ and $\text{C}_6\text{H}_5\text{C}_2\text{H}_3 = \text{C}_6\text{H}_6 + \text{H}_2\text{CC}$. Besides, the ring-rearrangement of methyl-cyclopentadienyl radical ($\text{C}_5\text{H}_4\text{CH}_3$), following the dissociation of xylyl radicals (o, m, and p- $\text{C}_8\text{H}_9 = \text{C}_5\text{H}_4\text{CH}_3 + \text{C}_2\text{H}_2$ [7–9]), also contribute to C_6H_6 production. The formation of toluene (C_7H_8) mainly relies on the ipso-substitution reactions of H+xylene (R8), and a minor part of C_7H_8 also comes from the hydrogen abstraction reaction from xylenes by benzyl (C_7H_7) and the $\text{C}_7\text{H}_7 + \text{H}$ recombination. The measurements and simulations consistently show that styrene ($\text{C}_6\text{H}_5\text{C}_2\text{H}_3$) starts to form at a lower temperature and has a higher peak mole fraction in o-xylene pyrolysis. This is mainly due to the fuel specific channel of $\text{o-C}_8\text{H}_8 \rightarrow \text{benzocyclobutene} (\text{C}_6\text{H}_4\text{C}_2\text{H}_4) \rightarrow \text{C}_6\text{H}_5\text{C}_2\text{H}_3$. The crucial intermediate $\text{C}_6\text{H}_4\text{C}_2\text{H}_4$ is identified and quantified in the current experiments, and the mole fraction profiles are shown in Fig. 7(d). The formation of $\text{C}_6\text{H}_4\text{C}_2\text{H}_4$ occurs at around 1200 K when the fuel just starts to decompose in o-xylene pyrolysis, while in the other two cases, $\text{C}_6\text{H}_4\text{C}_2\text{H}_4$ comes after the production of o-xylene as an intermediate. The measurements of ethylbenzene ($\text{C}_6\text{H}_5\text{C}_2\text{H}_5$) are less satisfactorily predicted, compared to other MAHs, by the kinetic model. ROP-analyzed results at 1400 K show that $\text{C}_6\text{H}_5\text{C}_2\text{H}_5$ mainly come from the $\text{C}_7\text{H}_7 + \text{CH}_3$ recombination, and this reaction carries on after the arrival of the quenching waves. By using the measured pressure profiles, the simulated mole fractions of $\text{C}_6\text{H}_5\text{C}_2\text{H}_5$ are enhanced, but still below the experimental results. It is noteworthy that the early formation of $\text{C}_6\text{H}_5\text{C}_2\text{H}_5$ is a unique feature in o-xylene pyrolysis, and a H-assisted isomerization reaction $\text{H} + \text{o-C}_8\text{H}_{10} = \text{H} + \text{C}_6\text{H}_5\text{C}_2\text{H}_5$ with an estimated rate coefficient of $5.0 \times 10^{11} \text{ cm}^3 \text{ mole}^{-1} \text{ s}^{-1}$ is included in the current model to match the measured $\text{C}_6\text{H}_5\text{C}_2\text{H}_5$ mole fractions at relatively low temperatures. Future experimental or theoretical works are needed to better account for this observation. The formation of phenylacetylene ($\text{C}_6\text{H}_5\text{C}_2\text{H}$) commences at a slightly lower temperature in o-xylene pyrolysis, compared to that in the other two cases. ROP-analyzed results show that the dissociation of $\text{C}_6\text{H}_5\text{CHCH}$ radical ($\text{C}_6\text{H}_5\text{CH}=\dot{\text{C}}\text{H}$) is the major source of $\text{C}_6\text{H}_5\text{C}_2\text{H}$, and the $\text{C}_6\text{H}_5\text{CHCH}$ radical originates from the consumption of the isomer pair $\text{C}_6\text{H}_5\text{C}_2\text{H}_3$ and $\text{C}_6\text{H}_4\text{C}_2\text{H}_4$.

Measured and simulated mole fraction profiles of C_1 – C_4 products are presented in Fig. 8. The current kinetic model can well predict the absolute concentrations as well as the relative abundance among the three cases. Speciation behaviors of these small species, especially regarding the temperature windows, are similar in the pyrolysis of the three xylene isomers, except for the higher

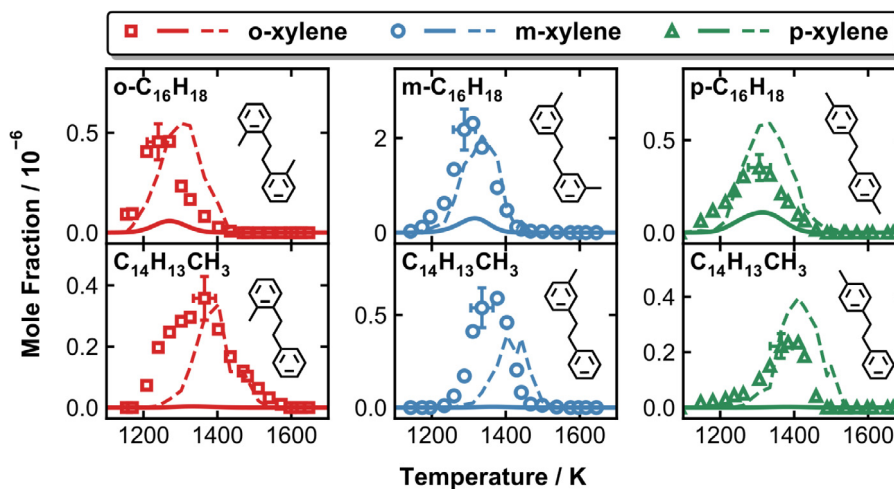


Fig. 9. Experimental (symbols) and simulated (lines) mole fraction profiles of fuel-specific $C_{16}H_{18}$ and $C_{15}H_{16}$ isomers in the pyrolysis of three xylene isomers. The solid lines are simulations based on constant pressure assumption over a nominal reaction time of 4.0 ms, and the dashed lines are simulations using measured pressure profiles up to 10 ms.

ethylene (C_2H_4) mole fractions in o-xylene pyrolysis. The current kinetic model attributes the C_2H_4 production mainly to the dissociation of $C_6H_4C_2H_4$ ($C_6H_4C_2H_4 = o-C_6H_4 + C_2H_4$), and also the $C_6H_5C_2H_3$ consumption via $C_6H_5C_2H_3 + H = C_6H_5 + C_2H_4$.

4.3. Formation and growth of polycyclic aromatic hydrocarbons (PAHs)

Specific PAHs, mainly isomers with the formulas of $C_{16}H_{18}$ and $C_{15}H_{16}$, that are closely related to the fuel consumption are observed at relatively low temperatures, as can be seen in Fig. 1. The product from the self-recombination of corresponding xylyl radical is supposed to be the most dominant $C_{16}H_{18}$ isomer in each case. In particular, 2,2'-dimethyl-bibenzyl (o- $C_{16}H_{18}$) and 4,4'-dimethyl-bibenzyl (p- $C_{16}H_{18}$) are identified through standards injection, as mentioned in the experimental section. The $C_{16}H_{18}$ peak appearing at 9.7 min, with an outstanding intensity in m-xylene pyrolysis (see Fig. 1), is confidently speculated to be 3,3'-dimethyl-bibenzyl (m- $C_{16}H_{18}$). The $C_{15}H_{16}$ peaks with the highest concentrations in separate cases are considered as methyl-bibenzyl (lumped as $C_{14}H_{13}CH_3$ in the kinetic model), which come from the recombination of the corresponding xylyl radical with benzyl. Measured and simulated mole fraction profiles of these fuel-specific species are presented in Fig. 9, and the chemical structures are also illustrated. Similar to the case of bibenzyl formation through benzyl self-recombination mentioned in our previous publications [31,33,34], the recombination reactions of resonance-stabilized radicals forming $C_{16}H_{18}$ and $C_{15}H_{16}$ continue during the post-shock quenching. Therefore, the use of measured pressure profiles is necessary to simulate their mole fractions as a function of the post-shock temperature T_5 . Simulations based on constant pressure (20 bar) assumption over the nominal reaction time of 4.0 ms and using measured pressure profiles are both shown in Fig. 9, and the majority of the shown species are actually formed after the arrival of the rarefaction waves. The kinetic model can satisfactorily predict the measurements, given a relatively large uncertainty from both identification and quantification processes. Noteworthy, m- $C_{16}H_{18}$ has four times higher concentrations than the o- and p-isomers in corresponding cases. The reason lies in that the self-recombination reaction is a more important sink for m-xylyl than for o- and p-xylyl under the same conditions, since m-xylyl does not undergo the hydrogen loss to form m-xylene. The formation of methyl bibenzyl ($C_{14}H_{13}CH_3$), compared to dimethyl bibenzyl (o-, m-, and p- $C_{16}H_{18}$) starts at a higher temperature, as it re-

quires the participation of benzyl. The *ipso*-substitution reaction o-, m- and p- $C_{16}H_{18} + H = C_{14}H_{13}CH_3 + CH_3$ has a negligible contribution to $C_{14}H_{13}CH_3$ production. Due to the higher concentration of m-xylyl compared to o- and p-xylyl (see Fig. 4), $C_{14}H_{13}CH_3$ has a higher peak mole fraction in m-xylene pyrolysis.

Other PAHs that are observed in the low temperature regime include anthracene ($AC_{14}H_{10}$) in o-xylene pyrolysis and a $C_{16}H_{16}$ peak with the retention time of 11.2 min in p-xylene pyrolysis (see Fig. 1). The $C_{16}H_{16}$ peak is unique in p-xylene pyrolysis at low temperatures, so it is unlikely to be dimethyl-styrene formed through dehydrogenation of p- $C_{16}H_{18}$. Parylenes (polymers of p-xylylene), which have been widely used for microelectronic and medical coating [55,56], was discovered in 1947 by Szwarc [57] among the thermal decomposition products of p-xylene above 1000 °C. The above-mentioned $C_{16}H_{16}$ species observed in this work is thus assumed to be a dimer of p- C_8H_8 , (p- C_8H_8)₂. An indirect evidence is that compared to o-xylene and m-xylene, fewer peaks with relatively lower intensities are seen in p-xylene pyrolysis at around 1300 K, as can be noted in Fig. 1. This suggests that a larger part of carbon is converted to species that cannot be detected using the current experimental techniques, more specifically for this case, the larger polymers of p- C_8H_8 . Figure 10 presents the mole fraction profiles of $AC_{14}H_{10}$ in the pyrolysis of three xylenes and (p- C_8H_8)₂ in p-xylene pyrolysis. The speciation of $AC_{14}H_{10}$ in o-xylene pyrolysis is distinct from that in the other two studied cases: both the onset and the peak temperatures are obviously lower and the peak concentration is about 1.5 times higher. Such phenomena indicate the existence of fuel-specific $AC_{14}H_{10}$ formation pathways in o-xylene pyrolysis. In the current kinetic model, two lumped reactions, starting from o- $C_8H_9 + o-C_8H_9$ and o- $C_8H_9 + C_7H_7$, respectively (R20 and R21) are proposed to explain the early formation of $AC_{14}H_{10}$. The kinetic parameters used in the model are estimated to match the measurements. Future theoretical calculations are needed to know the exact detailed processes. The $AC_{14}H_{10}$ mole fraction profiles in three cases are more similar for the decreasing phase. At elevated temperatures, $AC_{14}H_{10}$ mainly isomerizes to phenanthrene ($PC_{14}H_{10}$) or undergoes hydrogen abstraction reaction by H atom. The current model includes the polymerization reactions of p- C_8H_8 forming the polymers containing up to five units. The simulation matches well with the measurement below 1400 K where (p- C_8H_8)₂ concentration increases with the temperature. The less satisfactory prediction at higher temperatures may be due to missing consumption pathways of (p- C_8H_8)₂.

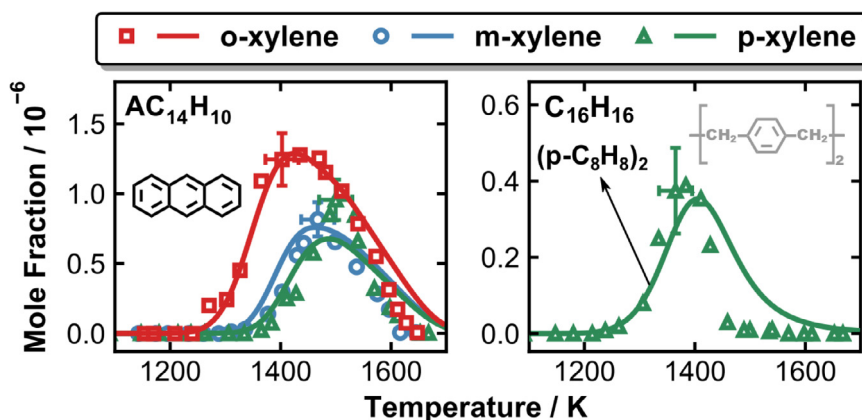


Fig. 10. Experimental (symbols) and simulated (lines) mole fraction profiles of anthracene ($AC_{14}H_{10}$) in the pyrolysis of three xylenes and $C_{16}H_{16}$ species (potentially ($p-C_8H_8$)₂) in p-xylene pyrolysis.

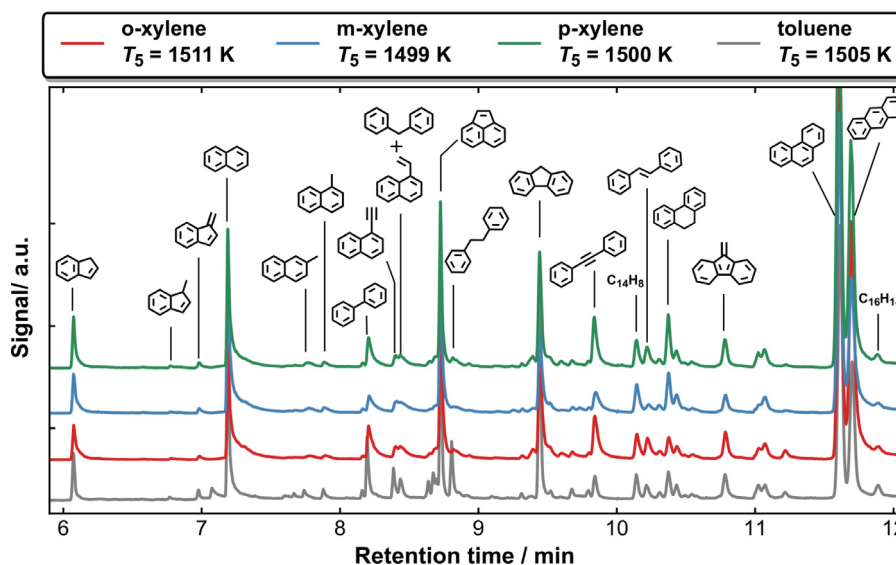


Fig. 11. GC signals for PAH species in the pyrolysis of three xylenes and toluene [35] with initial fuel concentrations of 100 ppm at the temperature around 1500 K.

The speciation of fused PAHs usually occurs at relatively high temperatures, in most cases above 1400 K, according to experimental observations in our previous works. Figure 11 compares the GC signals of PAH species in the pyrolysis of three xylenes at around 1500 K, and the signal recorded in 100 ppm toluene pyrolysis [35] is also shown as a reference. It is seen that the types and abundance of the PAH species at 1500 K are very similar among the pyrolysis of three xylenes and toluene. This suggests that the reaction schemes of PAH formation and growths are highly similar at elevated temperatures where the fuel chemistry has no obvious effects. In comparison to toluene, two major differences can be noticed in xylenes pyrolysis: first, bibenzyl concentrations are much lower; second the $AC_{14}H_{10}/PC_{14}H_{10}$ ratios are higher.

Mole fraction profiles of the PAHs that have not been discussed above, mostly fused PAHs that are observed in the pyrolysis of all three xylenes, are presented in Fig. 12. Naphthalene ($C_{10}H_8$) is found as the most abundant PAH products in the pyrolysis of o-xylene and p-xylene, while in the case of m-xylene pyrolysis, it has a comparable peak concentration with 3,3'-dimethylbibenzyl ($m-C_{16}H_{18}$). Other major PAHs with peak mole fractions above 1 ppm include indene (C_9H_8), acenaphthalene ($C_{12}H_8$) and phenanthrene ($C_{14}H_{10}$). Overall, most PAH mole fraction profiles have similar shapes and sizes among the three studied cases, though specific PAHs, such as bibenzyl ($C_6H_5C_2H_4C_6H_5$) and stil-

bene ($C_6H_5C_2H_2C_6H_5$), have obviously higher concentrations in o-xylene pyrolysis. The current kinetic model satisfactorily reproduces the measurements for most shown PAHs simply based on the constant pressure assumption. For the PAHs whose formation largely proceeds during the post-shock quenching, specifically, $C_6H_5C_2H_4C_6H_5$ and 1-methyl indene ($C_9H_7CH_3-1$), the measured pressure profiles are used to simulate their mole fractions as a function of the temperature. Modeling analyses are used to map out the PAH formation reaction pathways, as presented in Fig. 13, to assist the following discussion on the PAH speciation behaviors in the pyrolysis of xylenes. The ROP analyses are performed at T_5 of 1500 K where most PAHs have considerable mole fractions.

C_8 species, more specifically styrene ($C_6H_5C_2H_3$), benzocyclobutene ($C_6H_4cC_2H_4$) and phenylacetylene ($C_6H_5C_2H$), play an essential role in the PAH formation chemistry. This can be seen from different aspects: first, the isomerization of 1-phenylpropyne ($C_6H_5C_3H_3P_1$) which is formed from the reaction between $C_6H_5C_2H$ and CH_3 , dominates the production of indene (C_9H_8), while the efficient and direct C_9H_8 formation pathway through $C_7H_7+C_2H_2$ has the second largest contribution. Apart from the C_8+C_1 and C_7+C_2 pathways, a C_6+C_3 channel via an intermediate phenyl-allene ($C_6H_5C_3H_3A$) also leads to a small part of C_9H_8 . To point out, the relative importance of these three pathways does not vary much among the three studied cases, though $C_6H_5C_2H_3$

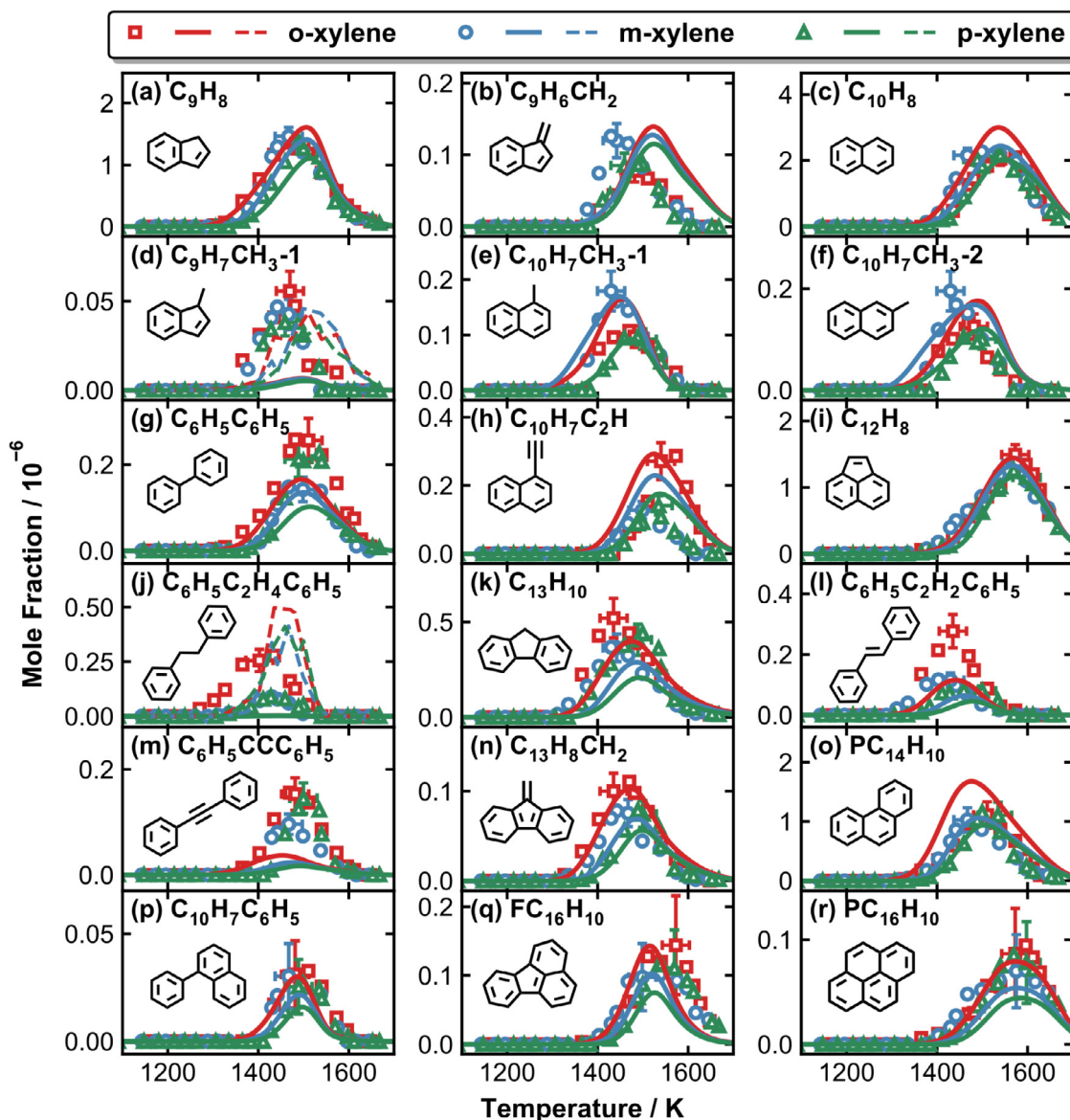


Fig. 12. Experimental (symbols) and simulated (lines) mole fraction profiles for shared PAH products observed in the pyrolysis of three xylenes. The solid lines are simulations based on constant pressure assumption over a nominal reaction time of 4.0 ms, and the dashed lines are simulations using measured pressure profiles up to 10 ms.

and $C_6H_4C_2H_4$ have higher concentrations in o-xylene pyrolysis. Besides, phenyl (C_6H_5), a crucial aromatic radical in the PAH formation scheme, mainly comes from the dissociation of $C_6H_5C_2H_3$. Furthermore, towards the formation of benzofulvene ($C_9H_6CH_2$), an essential precursor of naphthalene ($C_{10}H_8$), the Hydrogen-Abstraction- C_2H_2 -Addition (HACA) route of $C_6H_4C_2H + C_2H_2$ leading to the benzofulvenyl radical (C_9H_6CH) plays a predominant role, especially in o-xylene pyrolysis. Other sources of $C_9H_6CH_2$ mainly include the stepwise hydrogen loss of 1-methylindene ($C_9H_7CH_3-1$) formed via indenyl (C_9H_7)+ CH_3 recombination as well as the reaction of fulvenallene (C_7H_5)+propargyl (C_3H_3). The formation of naphthalene ($C_{10}H_8$) largely relies on the stabilization of naphthyl radicals ($C_{10}H_7-1$ and $C_{10}H_7-2$), following the $C_6H_4C_2H + C_2H_2$ and $C_6H_5 + C_4H_2$ reactions, in the pyrolysis of xylenes. Other pathways to naphthalene include the isomerization of benzofulvene ($C_9H_6CH_2$) and the dehydrogenation/isomerization of 1-methylindene ($C_9H_7CH_3-1$) as well as the cycloaddition fragmentation involving o-benzyne + benzene through the BICYCLO intermediate [53]. Naphthalene as well as its radicals further react with other radicals/molecules in the species pool, resulting in other

PAHs with a naphthalene core, such as methyl-naphthalene isomers ($C_{10}H_7CH_3-1$, $C_{10}H_7CH_3-2$), ethynyl-naphthalene ($C_{10}H_7C_2H$) and 1-phenyl naphthalene ($C_{10}H_7C_6H_5$). Despite relatively low concentrations, the mentioned species are identified and quantified in the current experiments, as shown in Fig. 12, and the kinetic model give satisfactory predictions. The HACA route via $C_{10}H_7-1 + C_2H_2$ also leads to around 10% of acenaphthalene ($C_{12}H_8$) formation in each case, while the predominant formation channel of $C_{12}H_8$ is through the $C_9H_7 + C_3H_3$ recombination and the subsequent dehydrogenation and isomerization. The mole fraction profiles of $C_{12}H_8$ are highly similar among the three cases, since the speciation of $C_{12}H_8$ occurs at relatively high temperatures where the fuel chemistry has negligible influences. Benzyl (C_7H_7) is also a crucial radical controlling the PAH formation in the pyrolysis of xylenes. At the analyzed temperature of 1500 K, C_7H_7 mainly comes from the consumption of toluene via hydrogen abstraction reactions by H and CH_3 , the isomerization of methyl phenyl ($CH_3C_6H_4$), as well as the addition of CH_3 to benzyne (o- C_6H_4) (these reaction pathways are not shown in Fig. 13). As mentioned above, C_7H_7 reacts with C_2H_2 directly forming C_9H_8 , and the self-recombination and the re-

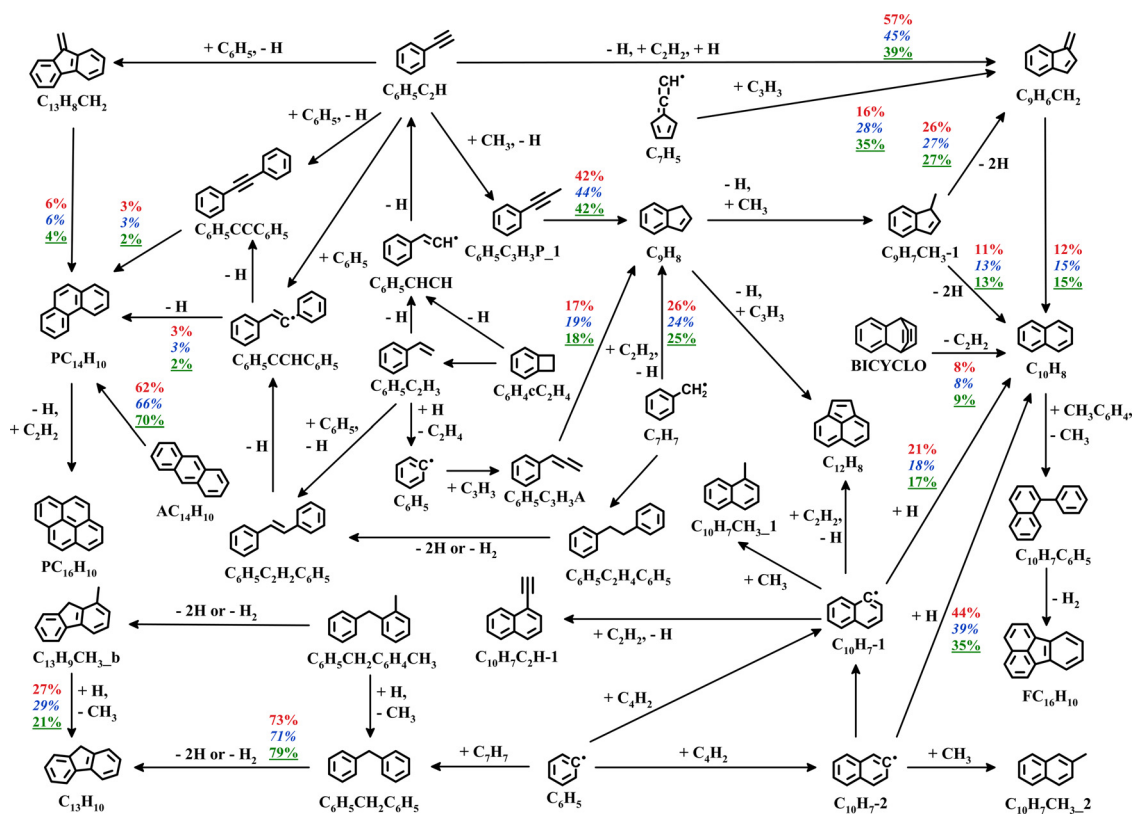


Fig. 13. Reaction pathways for PAH formation at $T_5 = 1500$ K in the pyrolysis of xylenes based on ROP analyses. The numbers (normal for o-xylene, italic for m-xylene and underlined for p-xylene) represent the percentage contributions of corresponding reactions to the PAHs on the arrow direction.

combination with xylyl radicals result in bibenzyl ($C_6H_5C_2H_4C_6H_5$) and methyl bibenzyl ($C_{14}H_{13}CH_3$), Fig. 9, pathway not shown in Fig. 13), respectively. Biphenyl methane ($C_6H_5CH_2C_6H_5$), which is the major precursor of fluorene ($C_{13}H_{10}$), comes from the $C_7H_7 + C_6H_5$ recombination, similar to the case of toluene pyrolysis [31,34]. An alternative formation pathway of $C_{13}H_{10}$ in the pyrolysis of xylenes is through the *ipso*-substitution of 1-methyl-fluorene ($C_{13}H_9CH_3_b$) which originates from the xylyl+ C_6H_5 recombination. The stepwise dehydrogenation of $C_6H_5C_2H_4C_6H_5$ gives rise to a small part of stilbene ($C_6H_5C_2H_2C_6H_5$) and diphenylacetylene ($C_6H_5CCC_6H_5$), which mostly comes from the addition-elimination reactions of $C_6H_5 + C_6H_5C_2H_3$ and $C_6H_5 + C_6H_5C_2H$, respectively. The *ipso*-substitution reactions of methyl and dimethyl stilbene ($C_{16}H_{16}$ and $C_{14}H_{11}CH_3$) are considered in the current model (see Scheme 1), but are found not to obviously contribute to $C_6H_5C_2H_2C_6H_5$ formation. The kinetic model can accurately predict the observation that $C_6H_5C_2H_2C_6H_5$ has a much higher abundance in o-xylene pyrolysis than in the other two cases although the model underpredicts the experimental mole fractions. Sensitivity analyses for $C_6H_5C_2H_2C_6H_5$ in separate cases at the temperature of 1450 K are presented in Fig. S4. In each case, the addition-elimination reaction $C_6H_5C_2H_3 + C_6H_5 = C_6H_5C_2H_2C_6H_5 + H$ and the dehydrogenation of o- C_8H_9 forming o- C_8H_8 have large significant sensitivity coefficients, facilitating the formation of $C_6H_5C_2H_2C_6H_5$. In the pyrolysis of m- and p-xylenes, the isomerization of m- and p- C_8H_9 to o- C_8H_9 is found among the most sensitive reactions, as in all three cases, the formation of $C_6H_5C_2H_3$, the main precursor of $C_6H_5C_2H_2C_6H_5$, depends upon the reaction sequence of o- $C_8H_9 \rightarrow$ o- $C_8H_8 \rightarrow C_6H_4cC_2H_4 \rightarrow C_6H_5C_2H_3$. This accounts for the higher $C_6H_5C_2H_2C_6H_5$ production in o-xylene pyrolysis. According to the analyzed results with the current model, the $C_6H_5 + C_6H_5C_2H$ addition-elimination reactions, directly or via the isomers $C_6H_5CCC_6H_5$ and 9-methylene-fluorene ($C_{13}H_8CH_2$) as in-

termediates, are a source of phenanthrene ($PC_{14}H_{10}$). These reactions were included in our study on phenylacetylene pyrolysis, as the three $C_{14}H_{10}$ isomers ($C_6H_5CCC_6H_5$, $C_{13}H_8CH_2$ and $PC_{14}H_{10}$) were observed among the major PAH products related to fuel consumption [32]. A recent theoretical study showed that the $C_6H_5 + C_6H_5C_2H$ predominantly forms $C_6H_5CCC_6H_5$ whose further isomerization to $PC_{14}H_{10}$ however lacks of theoretical evidence [58]. The isomerization of $AC_{14}H_{10}$ is found as a more significant pathway of $PC_{14}H_{10}$. The reason lies in the fact that $AC_{14}H_{10}$ is among the primary products that are directly formed through the initial decomposition steps of o-xylene which is also present as an intermediate in the pyrolysis of m- and p-xylenes. The four ring PAH isomers pyrene ($PC_{16}H_{10}$) and fluoranthene ($FC_{16}H_{10}$) starts to form above 1400 K, thus the fuel chemistry has limited effects and similar concentrations are observed among the three studied cases. The formation of $FC_{16}H_{10}$ is dominated by the dehydrogenation of $C_{10}H_7C_6H_5$ while $PC_{16}H_{10}$ mainly comes from the HACA route via phenanthryl ($PC_{14}H_9$)+ C_2H_2 .

5. Conclusions

A comparative study on the pyrolysis of three xylene isomers is carried out in this work via a combination of shock tube experiments and kinetic modeling analyses. Post-shock mixtures are sampled and analyzed using GC/GC-MS techniques, yielding species mole fractions as a function of the post-shock temperature. A sub-mechanism for xylenes, which incorporates theoretically determined rate coefficients for the reactions of individual xylenes as well as uniform rate rules for all three isomers, is developed based on our on-going PAH formation kinetic model. The kinetic model can satisfactorily reproduce the measurements, regarding the fuel decomposition reactivity and the speciation of various products ranging from small molecules to up to four ring

PAHs. The three xylene isomers exhibit similar decomposition reactivity, which falls between that of toluene and ethylbenzene. The slightly slower consumption of *m*-xylene, in comparison to the *o*- and *p*- isomers, lies in the fact that the *m*-xylyl radical cannot undergo the dehydrogenation leading to *m*-xylylene. Different species pools are observed at relatively low temperatures where the initial fuel decomposition steps occur, which is attributed to the different fates of the three xylyl radicals. More specifically, dehydrogenation of *o*-xylyl and *p*-xylyl leads to the formation of *o*-xylylene and *p*-xylylene, respectively, while *m*-xylyl is consumed mainly via the isomerization to *o*-xylyl. The further consumption of *o*-xylylene produces a considerable amount of styrene, with the isomer benzocyclobutene being an intermediate. On the other hand, *p*-xylylene undergoes polymerization processes, as suggested by indirect experimental evidence. Due to a smaller removal rate, *m*-xylyl has a higher abundance, and therefore 3,3'-dimethylbibenzyl produced from *m*-xylyl self-recombination is observed of significant concentrations. Early formation of anthracene is noted as a unique feature in *o*-xylene pyrolysis, and lumped reactions of *o*-xylyl + benzyl and *o*-xylyl + *o*-xylyl are proposed to account for such a phenomenon. At elevated temperatures where the fuels are depleted, PAH speciation, regarding both types and amounts, are very similar in the pyrolysis of three xylenes. Since toluene is a major product in the decomposition of all three xylenes through *ipso*-substitution reactions, benzyl/toluene related pathways contribute to the formation of PAH species. Nevertheless, modeling analyses reveal that the chemistry of C₈ species such as styrene, styryl and phenylacetylene, plays a more essential role, especially in *o*-xylene pyrolysis.

Declaration of Competing Interest

The authors declare that they have no known competing financial interests or personal relationships that could have appeared to influence the work reported in this paper.

Acknowledgments

This project has received funding from the European Research Council (ERC) under the European Union's Horizon 2020 research and innovation program (grant agreement No. 756785).

Supplementary materials

Supplementary material associated with this article can be found, in the online version, at doi:10.1016/j.combustflame.2022.112247.

References

- [1] A. Violi, S. Yan, E. Eddings, A. Sarofim, S. Granata, T. Faravelli, E. Ranzi, Experimental formulation and kinetic model for JP-8 surrogate mixtures, *Combust. Sci. Technol.* 174 (2002) 399–417.
- [2] S.M. Sarathy, A. Farooq, G.T. Kalghatgi, Recent progress in gasoline surrogate fuels, *Prog. Energy Combust.* 65 (2018) 67–108.
- [3] W.J. Pitz, C.J. Mueller, Recent progress in the development of diesel surrogate fuels, *Prog. Energy Combust.* 37 (2011) 330–350.
- [4] J. Emdee, K. Brezinsky, I. Glassman, Oxidation of *o*-xylene, *Proc. Combust. Inst.* 23 (1991) 77–84.
- [5] J. Emdee, K. Brezinsky, I. Glassman, High-temperature oxidation mechanisms of *m*- and *p*-xylene, *J. Phys. Chem.* 95 (1991) 1626–1635.
- [6] W. Yuan, L. Zhao, S. Gail, J. Yang, Y. Li, F. Qi, P. Dagaut, Exploring pyrolysis and oxidation chemistry of *o*-xylene at various pressures with special concerns on PAH formation, *Combust. Flame* 228 (2021) 351–363.
- [7] S. Gail, P. Dagaut, Experimental kinetic study of the oxidation of *p*-xylene in a JSR and comprehensive detailed chemical kinetic modeling, *Combust. Flame* 141 (2005) 281–297.
- [8] S. Gail, P. Dagaut, Oxidation of *m*-xylene in a JSR: experimental study and detailed chemical kinetic modeling, *Combust. Sci. Technol.* 179 (2007) 813–844.
- [9] S. Gail, P. Dagaut, G. Black, J.M. Simmie, Kinetics of 1, 2-dimethylbenzene oxidation and ignition: experimental and detailed chemical kinetic modeling, *Combust. Sci. Technol.* 180 (2008) 1748–1771.
- [10] F. Battin-Leclerc, R. Bounaceur, N. Belmekki, P. Glaude, Experimental and modeling study of the oxidation of xylenes, *Int. J. Chem. Kinet.* 38 (2006) 284–302.
- [11] S. Gudiyella, T. Malewicki, A. Comandini, K. Brezinsky, High pressure study of *m*-xylene oxidation, *Combust. Flame* 158 (2011) 687–704.
- [12] H.-P.S. Shen, M.A. Oehlschlaeger, The autoignition of C₈H₁₀ aromatics at moderate temperatures and elevated pressures, *Combust. Flame* 156 (2009) 1053–1062.
- [13] G. Kukkadapu, D. Kang, S.W. Wagnon, K. Zhang, M. Mehl, M. Monge-Palacios, H. Wang, S.S. Goldsborough, C.K. Westbrook, W.J. Pitz, Kinetic modeling study of surrogate components for gasoline, jet and diesel fuels: C7–C11 methylated aromatics, *Proc. Combust. Inst.* 37 (2019) 521–529.
- [14] A. Roubaud, O. Lemaire, R. Minetti, L. Sochet, High pressure auto-ignition and oxidation mechanisms of *o*-xylene, *o*-ethyltoluene, and *n*-butylbenzene between 600 and 900K, *Combust. Flame* 123 (2000) 561–571.
- [15] A. Roubaud, R. Minetti, L. Sochet, Oxidation and combustion of low alkylbenzenes at high pressure: comparative reactivity and auto-ignition, *Combust. Flame* 121 (2000) 535–541.
- [16] Y. Li, L. Zhang, T. Yuan, K. Zhang, J. Yang, B. Yang, F. Qi, C.K. Law, Investigation on fuel-rich premixed flames of monocyclic aromatic hydrocarbons: part I. Intermediate identification and mass spectrometric analysis, *Combust. Flame* 157 (2010) 143–154.
- [17] C. Ji, E. Dames, H. Wang, F.N. Egolfopoulos, Propagation and extinction of benzene and alkylated benzene flames, *Combust. Flame* 159 (2012) 1070–1081.
- [18] L. Zhao, Z. Cheng, L. Ye, F. Zhang, L. Zhang, F. Qi, Y. Li, Experimental and kinetic modeling study of premixed *o*-xylene flames, *Proc. Combust. Inst.* 35 (2015) 1745–1752.
- [19] W. Yuan, L. Zhao, J. Yang, Z. Zhou, Y. Li, F. Qi, Insights into the decomposition and oxidation chemistry of *p*-xylene in laminar premixed flames, *J. Phys. Chem. A* 125 (2021) 3189–3197.
- [20] L. Dupont, H.Q. Do, G. Capriolo, A.A. Konnov, A. El Bakali, Experimental and kinetic modeling study of para-xylene chemistry in laminar premixed flames, *Fuel* 239 (2019) 814–829.
- [21] D. Han, S. Deng, W. Liang, P. Zhao, F. Wu, Z. Huang, C.K. Law, Laminar flame propagation and nonpremixed stagnation ignition of toluene and xylenes, *Proc. Combust. Inst.* 36 (2017) 479–489.
- [22] T. Bierkandt, P. Hemberger, P. Oßwald, M. Köhler, T. Kasper, Insights in *m*-xylene decomposition under fuel-rich conditions by imaging photoelectron photoion coincidence spectroscopy, *Proc. Combust. Inst.* 36 (2017) 1223–1232.
- [23] P. Hemberger, A.J. Trevitt, E. Ross, G. da Silva, Direct observation of para-xylylene as the decomposition product of the meta-xylyl radical using VUV synchrotron radiation, *J. Phys. Chem. Lett.* 4 (2013) 2546–2550.
- [24] P. Hemberger, A.J. Trevitt, T. Gerber, E. Ross, G. da Silva, Isomer-specific product detection of gas-phase xylyl radical rearrangement and decomposition using VUV synchrotron photoionization, *J. Phys. Chem. A* 118 (2014) 3593–3604.
- [25] G. da Silva, E.E. Moore, J.W. Bozzelli, Decomposition of methylbenzyl radicals in the pyrolysis and oxidation of xylenes, *J. Phys. Chem. A* 113 (2009) 10264–10278.
- [26] E. Dames, H. Wang, Isomerization kinetics of benzylic and methylphenyl type radicals in single-ring aromatics, *Proc. Combust. Inst.* 34 (2013) 307–314.
- [27] H. Hippler, S. Seisel, J. Troe, Pyrolysis of *p*-xylene and of 4-methylbenzyl radicals, *Proc. Combust. Inst.* 25 (1994) 875–882.
- [28] S. Lange, K. Luther, T. Rech, A. Schmoltner, J. Troe, CC and CH bond splits of laser-excited aromatic molecules. 4. Specific rate constants and branching ratios for the dissociation of the xylenes, *J. Phys. Chem.* 98 (1994) 6509–6513.
- [29] I. Da Costa, R. Eng, A. Gebert, H. Hippler, Direct observation of the rate of H-atom formation in the thermal decomposition of Ortho-, Meta-, and Para-xylene behind shock waves between 1300 and 1800K, *Proc. Combust. Inst.* 28 (2000) 1537–1543.
- [30] R.X. Fernandes, A. Gebert, H. Hippler, The pyrolysis of 2-, 3-, and 4-methylbenzyl radicals behind shock waves, *Proc. Combust. Inst.* 29 (2002) 1337–1343.
- [31] W. Sun, A. Hamadi, S. Abid, N. Chaumeix, A. Comandini, Probing PAH formation chemical kinetics from benzene and toluene pyrolysis in a single-pulse shock tube, *Proc. Combust. Inst.* 38 (2021) 891–900.
- [32] W. Sun, A. Hamadi, S. Abid, N. Chaumeix, A. Comandini, An experimental and kinetic modeling study of phenylacetylene decomposition and the reactions with acetylene/ethylene under shock tube pyrolysis conditions, *Combust. Flame* 220 (2020) 257–271.
- [33] W. Sun, A. Hamadi, S. Abid, N. Chaumeix, A. Comandini, A comparative kinetic study of C₈–C₁₀ linear alkylbenzenes pyrolysis in a single-pulse shock tube, *Combust. Flame* 221 (2020) 136–149.
- [34] W. Sun, A. Hamadi, S. Abid, N. Chaumeix, A. Comandini, Detailed experimental and kinetic modeling study of toluene/C₂ pyrolysis in a single-pulse shock tube, *Combust. Flame* 226 (2021) 129–142.
- [35] W. Sun, A. Hamadi, S. Abid, N. Chaumeix, A. Comandini, Influences of propylene/propyne addition on toluene pyrolysis in a single-pulse shock tube, *Combust. Flame* 236 (2022) 111799.
- [36] W. Sun, A. Hamadi, S. Abid, N. Chaumeix, A. Comandini, A comprehensive kinetic study on the speciation from propylene and propyne pyrolysis in a single-pulse shock tube, *Combust. Flame* 231 (2021) 111485.
- [37] X. Han, J.M. Mehta, K. Brezinsky, Temperature approximations in chemical kinetics studies using single pulse shock tubes, *Combust. Flame* 209 (2019) 1–12.
- [38] P.T. Lynch, C.J. Annesley, C.J. Aul, X. Yang, R.S. Tranter, Recombination of allyl radicals in the high temperature fall-off regime, *J. Phys. Chem. A* 117 (2013) 4750–4761.
- [39] J.A. Manion, D.A. Sheen, I.A. Awan, Evaluated kinetics of the reactions of H and CH₃ with *n*-alkanes: experiments with *n*-butane and a com-

- bustion model reaction network analysis, *J. Phys. Chem. A* 119 (2015) 7637–7658.
- [40] L.A. Mertens, J.A. Manion, β -bond scission and the yields of H and CH₃ in the decomposition of isobutyl radicals, *J. Phys. Chem. A* 122 (2018) 5418–5436.
- [41] A. Hamadi, W. Sun, S. Abid, N. Chaumeix, A. Comandini, An experimental and kinetic modeling study of benzene pyrolysis with C₂–C₃ unsaturated hydrocarbons, *Combust. Flame* 237 (2022) 111858.
- [42] W. Pejpichestakul, E. Ranzi, M. Pelucchi, A. Frassoldati, A. Cuoci, A. Parente, T. Faravelli, Examination of a soot model in premixed laminar flames at fuel-rich conditions, *Proc. Combust. Inst.* 37 (2019) 1013–1021.
- [43] S.J. Klippenstein, L.B. Harding, Y. Georgievskii, On the formation and decomposition of C₇H₈, *Proc. Combust. Inst.* 31 (2007) 221–229.
- [44] E. Zahedi, M. Mozaffari, L. Yousefi, A. Shiroudi, M.S. Deleuze, Kinetic and mechanistic study on the pyrolysis of 1, 3-dihydroisothianaphthene-2, 2-dioxide toward benzocyclobutene using RRKM and BET theories, *Chem. Phys.* 483 (2017) 12–25.
- [45] W. Tsang, J. Cui, Homogeneous gas-phase decyclization of tetralin and benzocyclobutene, *J. Am. Chem. Soc.* 112 (1990) 1665–1671.
- [46] L. Errede, F. DeMaria, The chemistry of xylylenes. XV. The kinetics of fast flow pyrolysis of p-xylene, *J. Phys. Chem.* 66 (1962) 2664–2672.
- [47] C. Silcocks, The kinetics of the thermal decomposition and polymerization of ethane and ethylene, *Proc. Math. Phys. Eng. Sci.* 233 (1956) 465–479.
- [48] A. Matsugi, A. Miyoshi, Kinetics of the self-reactions of benzyl and o-xylyl radicals studied by cavity ring-down spectroscopy, *Chem. Phys. Lett.* 521 (2012) 26–30.
- [49] L. Errede, J. Cassidy, The chemistry of xylylenes. V. The formation of anthracenes via fast flow pyrolysis of toluenes and related compounds², *J. Am. Chem. Soc.* 82 (1960) 3653–3658.
- [50] M. Colket, D. Seery, Reaction mechanisms for toluene pyrolysis, *Proc. Combust. Inst.* 25 (1994) 883–891.
- [51] A. Burcat, B. Ruscic, Third millennium ideal gas and condensed phase thermochemical database for combustion (with update from active thermochemical tables), Argonne National Lab.(ANL), Argonne, IL (United States), 2005.
- [52] E.R. Ritter, J.W. Bozzelli, THERM: thermodynamic property estimation for gas phase radicals and molecules, *Int. J. Chem. Kinet.* 23 (1991) 767–778.
- [53] COSILAB The Combustion Simulation Laboratory, Rotexo GmbH & Co., KG, Haan, Germany, 2009 Version 3.3.2.
- [54] W. Tang, K. Brezinsky, Chemical kinetic simulations behind reflected shock waves, *Int. J. Chem. Kinet.* 38 (2006) 75–97.
- [55] K. Pruden, K. Sinclair, S. Beaudoin, Characterization of parylene-N and parylene-C photooxidation, *J. Polym. Sci. A Polym. Chem.* 41 (2003) 1486–1496.
- [56] M. Cieřlik, M. Kot, W. Reczyński, K. Engvall, W. Rakowski, A. Kotarba, Parylene coatings on stainless steel 316L surface for medical applications—Mechanical and protective properties, *Mater. Sci. Eng. C* 32 (2012) 31–35.
- [57] M. Szwarc, Some remarks on the CH₂ [graphic omitted] CH₂ molecule, *Faraday Discuss.* 2 (1947) 46–49.
- [58] P. Liu, H. Jin, B. Chen, J. Yang, Z. Li, A. Bennett, A. Farooq, S. Mani Sarathy, W.L. Roberts, Rapid soot inception via α -alkynyl substitution of polycyclic aromatic hydrocarbons, *Fuel* 295 (2021) 120580.